



Article

# Technological Principles of Complex Plasma-Beam Surface Treatment of Al<sub>2</sub>O<sub>3</sub>/TiC and SiAlON Ceramics

Sergey N. Grigoriev <sup>1</sup>, Marina A. Volosova <sup>1,\*</sup>, Maxim A. Lyakhovetsky <sup>2</sup>, Artem P. Mitrofanov <sup>1</sup>,  
Nataliya V. Kolosova <sup>1</sup> and Anna A. Okunkova <sup>1</sup>

<sup>1</sup> Department of High-Efficiency Processing Technologies, Moscow State University of Technology “STANKIN”, Vadkovsky per., 3a, 127994 Moscow, Russia; s.grigoriev@stankin.ru (S.N.G.); a.mitrofanov@stankin.ru (A.P.M.); n.kapustina@stankin.ru (N.V.K.); a.okunkova@stankin.ru (A.A.O.)

<sup>2</sup> Department of Aircraft Engine Manufacturing Technology, Moscow Aviation Institute, Volokolamskoe Highway 4, 125993 Moscow, Russia; lyakhovetsky@yandex.ru

\* Correspondence: m.volosova@stankin.ru; Tel.: +7-499-972-94-29

**Abstract:** Thermomechanical action during high-performance diamond grinding of sintered cutting Al<sub>2</sub>O<sub>3</sub>/TiC and SiAlON ceramics leads to increased defectiveness of the surface layer of the deposited TiZrN and CrAlSiN/DLC coatings. It predetermines the discontinuous and porous coatings and reduces its effectiveness under abrasive exposure and fretting wear. The developed technological approach is based on “dry” etching with beams of accelerated argon atoms with an energy of 5 keV for high-performance removal of defects. It ensures the removal of the defective layer on ceramics and reduces the index of defectiveness (the product of defects’ density per unit surface area) by several orders of magnitude, compared with diamond grinding. There are no pronounced discontinuities and pores in the microstructure of coatings. Under mechanical loads, the coatings ensure a stable boundary anti-friction film between the ceramics and counter body that significantly increases the wear resistance of samples. The treatment reduces the volumetric wear under 20 min of abrasive action by 2 and 6 times for TiZrN and CrAlSiN/DLC coatings for Al<sub>2</sub>O<sub>3</sub>/TiC and by 5 and 23 times for SiAlON. The volumetric wear under fretting wear at 105 friction cycles is reduced by 2–3 times for both coatings for Al<sub>2</sub>O<sub>3</sub>/TiC and by 3–4 times for SiAlON.

**Keywords:** abrasive wear; Al<sub>2</sub>O<sub>3</sub>/TiC ceramics; defectiveness; fretting wear; plasma-beam treatment; SiAlON ceramics; surface layer; thin films; wear resistance



**Citation:** Grigoriev, S.N.; Volosova, M.A.; Lyakhovetsky, M.A.; Mitrofanov, A.P.; Kolosova, N.V.; Okunkova, A.A. Technological Principles of Complex Plasma-Beam Surface Treatment of Al<sub>2</sub>O<sub>3</sub>/TiC and SiAlON Ceramics. *J. Manuf. Mater. Process.* **2023**, *7*, 205. <https://doi.org/10.3390/jmmp7060205>

Academic Editors: Shrikant Joshi, Thomas Lampke and Thomas Lindner

Received: 13 October 2023  
Revised: 9 November 2023  
Accepted: 13 November 2023  
Published: 21 November 2023



**Copyright:** © 2023 by the authors. Licensee MDPI, Basel, Switzerland. This article is an open access article distributed under the terms and conditions of the Creative Commons Attribution (CC BY) license (<https://creativecommons.org/licenses/by/4.0/>).

## 1. Introduction

Solving the problems of increasing the wear resistance of machine parts and critical structural elements is among the most important for the further development of mechanical engineering. With the search for new materials and improvements in known structural and tool materials with an improved set of physical, mechanical, and operational properties, the opportunities for creating innovative mechanical engineering technologies and equipment are inextricably linked [1–3]. Structural steels and cast irons cannot compete with ceramics regarding hardness, heat resistance, and chemical inertness. Therefore, ceramics are increasingly used in various fields of mechanical engineering for the manufacture of cutting inserts and milling cutters for machining parts made of heat-resistant alloys and hardened steels, dies for the production of wire, bearing elements, nozzles for gas and plasma torches and spray devices, vacuum bushings devices, heating devices, pumps, etc. [4–8].

However, the share of industrial use of ceramics in the total global market for structural and tool materials is small despite all their known advantages [9,10]. The broader distribution of ceramics in the industry is hampered by their inherent disadvantages, such as primarily fragility and complexity in shaping processes [11,12]. The limitations of ceramics are especially pronounced when there is a combination of increased thermal and mechanical loads when accelerated microdestruction of the contact surfaces of ceramic

products is often observed. In the case of cyclic loads that occur during the operation of products, the probability of sudden microfracture is even higher [13–16]. The listed features are due to some factors—the structural heterogeneity of ceramics inherent in their nature, defects of a technological nature present in the volumetric structure and surface layer, which are inevitably formed during the sintering of powder compositions and subsequent diamond grinding of ceramic workpieces [17–20].

A separate scientific direction has been formed related to improving abrasive processing strategies, the characteristics of diamond tools, and optimizing diamond grinding modes to reduce roughness and increase crack resistance to solve the problem of minimizing defects in the surface layer of ceramic products [21–24]. One of the common approaches proposed by various researchers to reduce the defectiveness level in the surface layer formed on the surface of ceramics during diamond grinding is polishing as a finishing operation in the technological cycle of manufacturing ceramic products [25–27]. For example, the authors of this study demonstrated in a previous work that the use of additional finishing and polishing greatly reduces the index of defectiveness of the surface layer of samples made of  $\text{Al}_2\text{O}_3/\text{TiC}$  and  $\text{SiAlON}$  ceramics [28].

Another common technological approach among researchers to minimize surface layer defects and increase the wear resistance of ceramic products is the deposition of functional coatings such as  $\text{TiAlN}$ ,  $\text{TiZrN}$ ,  $\text{CrAlSiN}$ , etc. [29–35]. However, data obtained by various researchers show that increased defectiveness of the surface layer contributes to the formation of defective coatings with an increased content of pores and discontinuities, characterized by a reduced strength of the adhesive bond with the ceramic base, which significantly limits their effectiveness during operation [36–40]. A more detailed overview of the problem and the kind of defects is presented shortly in the previous work of the authors [28], where Section 2.1 is devoted to the detailed overview of the problem. The abovementioned issues indicate the need for pre-treatment ceramic products before coating deposition.

When the object of manufacture is ceramic products for the needs of aerospace and aviation, the performance characteristics of which are subject to the most stringent requirements, the most advanced and expensive technologies are used for their production [41–43]. Diamond grinding at high-performance modes is used in producing high-wear ceramic products in mass production with a relatively short service life (for example, cutting inserts and nozzles) to ensure high production profitability of expensive multi-axis sharpening equipment. In the production of these products, the design of which requires the processing of supporting surfaces, all kinds of chamfers and edges, polishing is impractical as a finishing operation from a technical and economic point of view. It is necessary to develop alternative approaches to solve such technological problems.

Thus, this work is the first to propose additional processing of industrially produced ceramic inserts using a non-contact plasma method without the expensive mechanical lapping and polishing, which includes multiple stages with reducing the wheel grain and individual approaches, which excludes the possibility of serial use of these operations to improve the quality of the surface of the inserts. The approach proposed by the authors is rational from the point of view of small-scale production, allowing us to process a series of ceramic cutting inserts in one operation using a plasma treatment unit and additional assets for their placement in the unit chamber, providing their simultaneous rotation.

This work aimed to develop and test the technological principles of complex plasma-beam surface treatment involving the removal of the defective ground layer and the deposition of functional coatings by the case of study of  $\text{Al}_2\text{O}_3/\text{TiC}$  and  $\text{SiAlON}$  ceramics that are common in the industry. When developing a new approach, we proceeded from a set of requirements related to ensuring high process productivity when processing ceramics of various chemical compositions, uniform processing of products with different design and geometric parameters, the absence of additional damaging effects on the surface layer, deterioration of the roughness of the product, and the possibility of combining the removal process of the defective layer in one technological operation with the deposition

of functional coatings such as TiZrN and CrAlSiN/DLC. For ceramic inserts made of  $\text{Al}_2\text{O}_3/\text{TiC}$  and SiAlON that are processed following the proposed principles, the index of defectiveness of the surface layer and wear resistance under abrasive and fretting wear were assessed.

## 2. Materials and Methods

### 2.1. Theoretical and Experimental Background

Multi-axis precision CNC grinding machines are used for diamond grinding (sharpening) of sintered ceramic workpieces as the finishing operation of a multi-stage technological process for manufacturing ceramic products in real production conditions. For example, in manufacturing ceramic cutting inserts, grinding of two opposite supporting surfaces is performed, followed by grinding the side surfaces, rounding the edges, and, if necessary, forming reinforcing chamfers [44]. Figure 1a illustrates an example of double-sided processing of round ceramic inserts with the end part of diamond grinding wheels on a dual-spindle surface grinding machine model WBM221 (Wendt GmbH, Auetal, Germany). In this case, the insert blanks are located in the recesses of a particular device (pallet) and fed into the processing zone. The lower and upper grinding wheels rotate with high cutting speeds (25–40 m/s), and the upper diamond wheel is simultaneously fed, providing an insertion force of the order of 10–15 N. The working part of the grinding wheels is equipped with a diamond-bearing cutting layer, which has a grain size of D64–D76 according to the FEPA standard. It should be noted that in processing the industrial cutting inserts by diamond grinding on the known type of production equipment and diamond wheels, a certain coolant was used in the production because the speeds and temperatures in the contact area are very high.

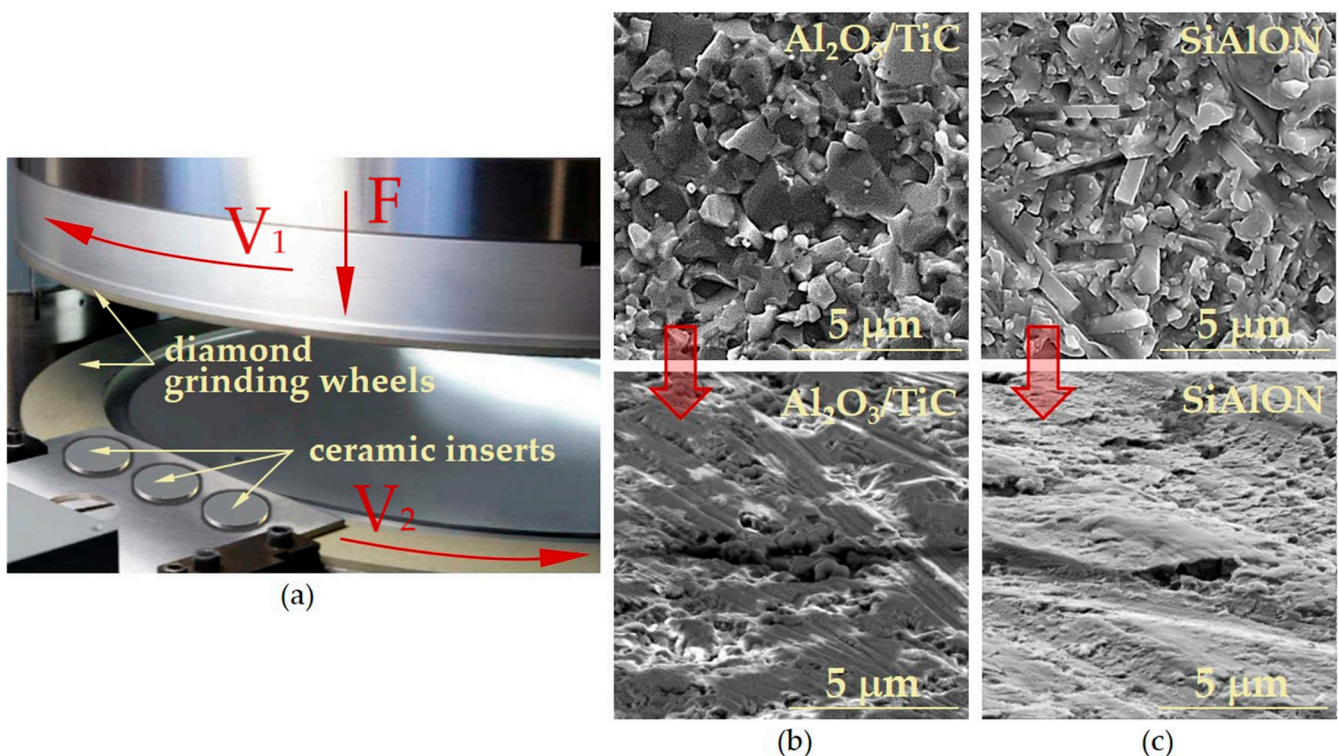


**Figure 1.** The process of double-sided diamond grinding of the supporting surfaces of round ceramic inserts (a), where  $F$  is the feed rate,  $V_1$  and  $V_2$  are the rotation velocities, and SEM images of the microstructure of the surface layer of inserts made of  $\text{Al}_2\text{O}_3/\text{TiC}$  (b) and SiAlON ceramics (c) after sintering (upper images) and diamond grinding (lower images).

During the diamond grinding under the described conditions, sintered ceramic workpieces are subjected to intense thermomechanical action. Consequently, the surface layer

is destroyed, and the required allowance (0.02–0.04 mm) is removed. In this case, the thermal and mechanical impact area is not limited by the size of the cut allowance but exceeds it [28,45,46]. Figure 1b,c illustrate the microstructure transformation of the surface layer of sintered ceramic workpieces made of  $\text{Al}_2\text{O}_3/\text{TiC}$  and SiAlON during diamond grinding. This transformation is a result of the impact of diamond grains and friction of the grinding wheel bond on the surface of the ceramic and plastic deformation under conditions of high-speed heating of local volumes of the ceramic material and subsequent cooling. Due to the increased thermomechanical loads acting on the ceramic workpiece during diamond grinding, the formed surface layer is characterized by increased defectiveness [28,47,48]. After diamond grinding, the surface layer has a typical microrelief, including sagging, grooves, microcracks, and craters from torn grains, as seen from the SEM images in Figure 1b,c.

Quantitative assessment of the microroughness of ceramic samples is carried out according to the ISO 21920-2:2021 standard, like for any other materials. The international standard includes various regulated parameters. As was shown in [28], the most informative parameter for assessing the condition of the surface layer of ceramics after diamond grinding is the total height of the profile (parameter  $R_t$ ). It is calculated as the sum of the greatest height of the protrusions of the profile and the greatest depth of the depressions of the profile within the length of the assessment along the OX axis. Thus, the value of the parameter  $R_t$  makes it possible to consider the surface layer defects mentioned above in calculations and is essentially the thickness of the defective layer. Figure 2 shows experimentally obtained profilograms of the surface layer of  $\text{Al}_2\text{O}_3/\text{TiC}$ - and SiAlON-ceramic inserts after diamond grinding. It can be seen that the microroughness profile of the two ceramic materials under study after grinding is represented by numerous protrusions and depressions, reflecting the defects, and the total depth of the defective layer within the assessment length reaches about 3.2  $\mu\text{m}$  for  $\text{Al}_2\text{O}_3/\text{TiC}$  and 2.1  $\mu\text{m}$  for SiAlON.

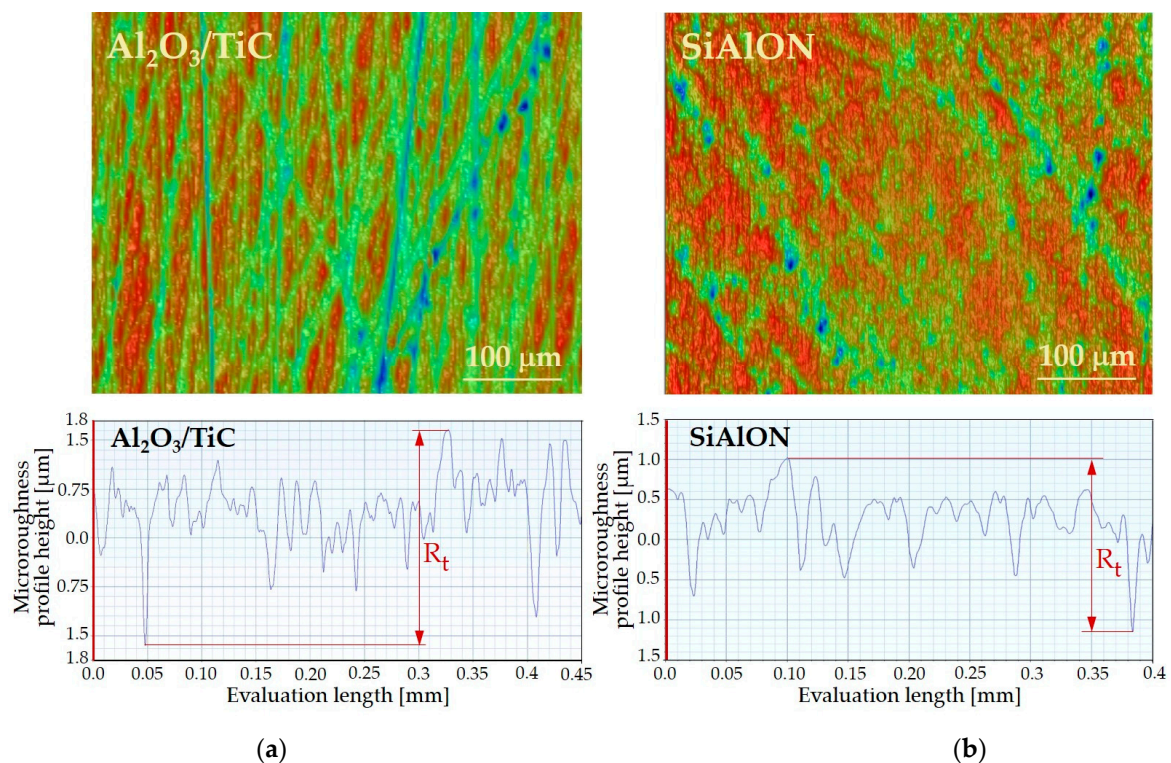


**Figure 2.** Profilograms of the surface layer of  $\text{Al}_2\text{O}_3/\text{TiC}$  (a) and SiAlON (b) ceramic inserts after diamond grinding: top view (upper image) and surface profile along the OX axis (lower image).

It should be noted that among different roughness parameters, the  $S_a$  roughness parameter is an obvious one at first glance concerning the proposed approach, with a few exceptions. The surface of the ceramic cutting insert after diamond grinding is characterized only by obvious protrusions, as well as by the profile of torn grains from their adhesion to the diamond wheel. The  $R_a$  parameter takes into account this feature of surface morphology. However,  $R_a$  is still the average distance between the protrusions and recesses. It is important for the overall surface quality assessment after diamond grinding, and we measure it. However, it does not provide objective data on the thickness of the defective layer. Therefore, the focus of this study is on assessing the parameter  $R_t$ , the distance between the maximum protrusion and depression, providing objective and complete data on the thickness of the defective layer.

The defective surface layer of a ceramic product, which is in contact with the counter body and perceives the entire complex of operational loads, has a predominant effect on friction and wear processes. It is known that microstructural defects are always stress concentrators [49,50]. When intense thermomechanical loads are applied, the defects present on the surface are likely the places where accelerated microdestruction of the contact surfaces of ceramic products begins. Therefore, there is reason to assume that various technological approaches aimed at minimizing or completely removing the defective layer formed during diamond grinding (as an alternative to expensive finishing and polishing) can potentially increase the wear resistance of products made from various ceramics. In addition, it can be expected that minimizing the level of defects in the surface layer will create favorable conditions for the functioning of subsequently deposited coatings on the contact areas of ceramic products [51–53].

When developing a technological approach for the effective removal of a defective layer, the authors of this work proceeded from a set of requirements related to the following:

- Ensuring high productivity in the processing of ceramics of various chemical compositions.
- Uniform processing of products with different design and geometric parameters.
- The absence of additional damaging effects on the surface layer and deterioration of the product roughness.
- The possibility of combining the process of removing a defective layer with the deposition of functional coatings into one technological operation.

The possibilities of using jet mechanical processing in air and water environments using microparticles of electro-corundum, electron beam exposure, and etching in vacuum-arc discharge plasma were studied [54–57]. It was experimentally established that those types of influence have an additional shock or thermal effect on the underlying sublayers and introduce their own defects simultaneously with removing the defective layer formed during diamond grinding. In addition, an increase in the surface roughness of ceramic products was found compared to the  $R_a$  parameter achieved by traditional diamond grinding (especially typical for jet machining).

The authors suggested that for the controlled removal of a thin defective layer from the surface of ceramic products, physical processes (without intense temperature heating and mechanical action) can be used, which are based on the energy impact of directed flows of electrons, ions or neutral particles generated by various energy sources. A source of beams of accelerated ions and fast atoms of inert gases (argon) generated by low-temperature plasma of a glow discharge was chosen as a source of energy impact [58–61].

The proposed technological approach for removing a defective layer of the surface of ceramic products after grinding by exposure to a beam of argon atoms is based on physical sputtering—the process of destruction of the surface layer of solids caused by particle bombardment. High-energy argon atoms bombarding the surface layer of ceramic samples lead to the displacement of atoms of the material under processing from the nodes of the crystal lattice and transfer a part of their energy to them. The primary displaced atoms either leave the surface of the ceramic sample or penetrate deep into the material and produce secondary knocked-out atoms, forming a cascade of displacements (collisions). As a result of the chaotic nature of the collision processes in the cascade, some atoms receive

momentum in the opposite direction, i.e., to the surface of the ceramic sample, and break away from it when their energy is higher than the energy of the near-surface bond. Thus, particles knocked out by argon atoms in a cascade of collisions of ceramic material atoms form a stream of sputtered particles. It should be emphasized that there is no chemical mechanism during the interaction of argon atoms with the surface of ceramic samples because bombardment is carried out with particles of inert gas that do not interact with the ceramic substrate material. Due to the possibility of varying processing parameters over a wide range (primarily the energy of particles bombarding the surface layer), it is possible to use this approach to solve a wide range of technological problems.

The mechanism for removing the surface layer by repeated exposure to bombarding argon atoms having a diameter of about 0.4 nm, knocking out particles from the surface of ceramic samples, is radically different from the impact of diamond grains on a grinding wheel, which occurs when removing allowance from ceramic workpieces and leading to the formation of a surface layer with a high level of defectiveness. Argon atoms, bombarding the ceramic material and gradually sputtering its surface layer, ensure the removal of the defective layer and its polishing. It should be noted that the proposed plasma treatment does not require technological allowance and allows the removal of the material in the tolerance range of diamond grinding. It removes about 5–6  $\mu\text{m}$  during the process, which is included in the tolerance for the final dimensions of the cutting insert taken into account when diamond grinding the inserts in real production.

A complex effect is provided on their surface layer, including bombardment (etching) of the defective layer with fast argon atoms and subsequent deposition of functional coatings on the “defect-free” surface layer following the proposed technological approach of plasma-beam surface treatment of products made of various ceramics. Figure 3 provides a schematic representation of the main stages of the proposed technological approach. At Stage 1, the defective layer is bombarded with fast argon atoms. At Stage 2, microparticles are sputtered (essentially knocked out) from the ceramic surface layer to the required depth. At Stage 3, the surface of the “defect-free” layer of ceramic products is activated by low-energy argon atoms to ensure better adhesion bond strength of the subsequently formed coating (for example, CrAlSiN), and Cr, Al, and Si particles evaporated from the surface of the cathode material (or sputtered from the target) interact with reaction gas (nitrogen) present in the atmosphere of the vacuum chamber, as a result of which the condensation process begins and the growth of the coating of the required thickness (Stage 4).

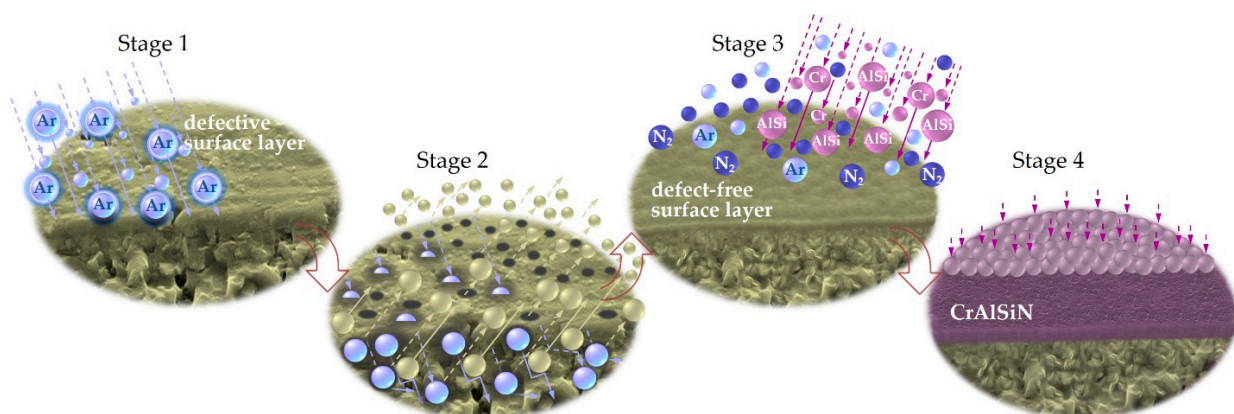


**Figure 3.** Schematic representation of the main stages of the technological process of complex plasma-beam surface treatment of ceramic products, including etching with beams of accelerated argon particles and deposition of functional coatings.

It should be noted that scaling the proposed approach at the industrial level is possible and includes issues mainly of design and technological character. For example, specialized equipment is required for serial application that would ensure the placement of multiple

cutting inserts in the setup chamber and their rotation during treatment, which would allow obtaining specific advantages in comparison with the same polishing that requires an individual approach, increasing costs many times.

## 2.2. Samples Made of $Al_2O_3/TiC$ and SiAlON Ceramics

Two types of ceramic inserts were used in the experimental studies (Figure 4a,b):

- Square inserts made of  $Al_2O_3/TiC$  ceramics with a width of 19.05 mm and a thickness of 7.94 mm; the phase composition of the material, obtained by analysis on an EMPYREAN X-ray diffractometer (PANalytical B.V., Almelo, the Netherlands), contains 71 vol.%  $Al_2O_3$ , 26 vol.% TiC, and 3 vol.%  $ZrO_2$ .
- Round-shaped inserts made of SiAlON ceramics with a diameter of 19.05 mm and a thickness of 7.94 mm; the phase composition of the material contains 79 vol.%  $Si_5AlON_7$ , 17 vol.%  $Si_3N_4$ , and 4 vol.%  $Yb_2O_3$ .

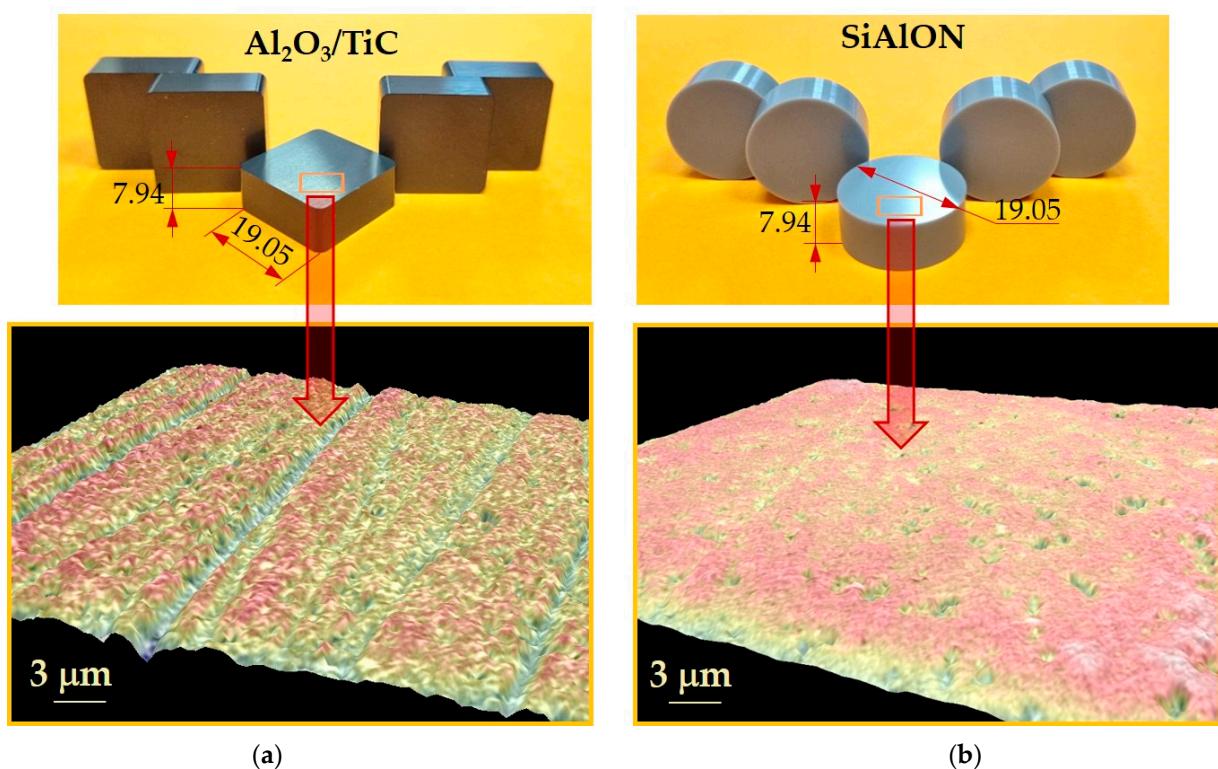


**Figure 4.** Samples of  $Al_2O_3/TiC$  (a) and SiAlON (b) ceramic inserts used in the experiments: general views of the inserts (upper image) and 3D profilograms of the surface layer (lower image).

Figure 4 shows 3D profilograms of the surface layer of  $Al_2O_3/TiC$  and SiAlON ceramics obtained on a Phenom G2 Pro scanning electron microscope (Phenom-World BV, Eindhoven, The Netherlands). It is seen that the surface layer of the original ceramic inserts after diamond grinding has the typical defects discussed in the previous section. Table 1 provides data on the main volumetric and surface characteristics of the ceramic samples used in the studies.

**Table 1.** Characteristics of the ceramic samples.

Type of Ceramics	Microhardness, GPa	Density, g/cm <sup>3</sup>	Fracture Toughness $K_{Ic}$ , MPa·m <sup>1/2</sup>	Roughness Parameter $R_a$ , μm	Total Height of Profile $R_t$ , μm
$Al_2O_3/TiC$	19.0	4.15	4.2	0.31	3.7
SiAlON	17.0	4.65	6.5	0.29	3.1

### 2.3. Processing Unit for Complex Plasma-Beam Surface Treatment of $Al_2O_3/TiC$ and SiAlON Ceramics

An experimental unit was created to implement the technological approach shown in Figure 3 and perform complex plasma-beam surface treatment of  $Al_2O_3/TiC$  and SiAlON ceramics. The general view of this unit is shown in Figure 5a. The processing of ceramic samples is carried out in a vacuum chamber made of stainless steel, shaped like a hexagonal prism (height is 85 cm, inscribed circle diameter is 60 cm). The unit has technological windows for mounting flanges with various equipment depending on the technological tasks to be solved. During the research, two magnetron systems with targets of different compositions were used: AlSi, Cr, and TiZr (Figure 5a,b). In addition, a source of beams of fast argon atoms was mounted on the left side flange of the vacuum chamber (Figure 5b). A rotary table with a planetary rotation system for processing ceramic samples is located on the lower base inside the vacuum chamber. The unit is equipped with a control stand to control and regulate the processing parameters.

Fast argon atoms passing through the grid of the beam source enter the unit chamber, the pressure of which is 0.2 Pa, and bombard the surface layer of the ceramic samples, sputtering it. Figure 5b shows a diagram illustrating its operating principle and a side view of the beam source. When the discharge voltage source is turned on, a glow discharge is ignited between the anode and the hull of the source located in the hollow cathode, which is the unit hull. An applied to the anode discharge voltage of 400 V and the discharge current of 2 A are used to maintain the discharge. During the experiments, a high negative voltage (−5 kV) was applied to the grid from a set of plates, as a result of which a grid layer was formed between the plasma and the grid, through which positive argon ions are drawn from the plasma towards the grid, which is under a negative potential. Ions passing through the blinds are neutralized by attaching electrons from the grid plates. The angle of contact with the plates is extremely small, so energy losses are minimal. After passing through the grid, neutral argon atoms entering the chamber of the technological unit, where the ceramic samples are placed, have energy of ~5 keV (the energy value was monitored by a spectrograph).

After removing the defective layer from the surface of ceramic samples, the unit performs activation of the surface of the samples with low-energy argon atoms (0.1–0.3 keV) and deposition of coatings of various compositions following the traditional principles of magnetron sputtering (or vacuum-arc evaporation with equipping the unit with evaporators), as well as gas-phase deposition of diamond-like carbon (DLC) coatings in a mixture of acetylene, tetramethylsilane, and argon.

### 2.4. Coating Deposition on Samples Made of $Al_2O_3/TiC$ and SiAlON Ceramics

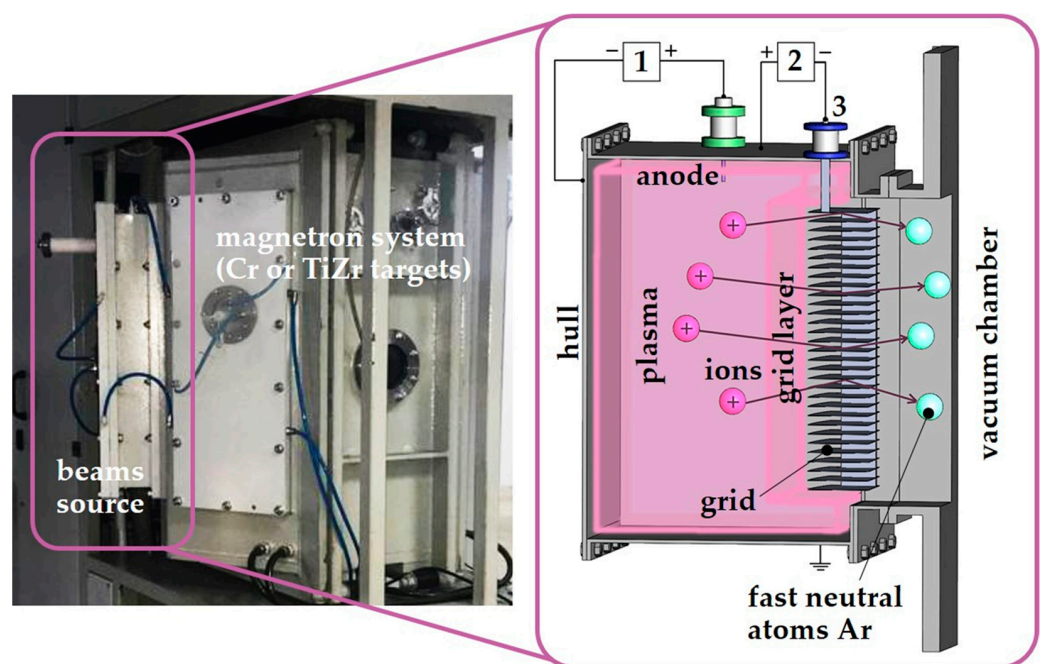
When choosing coating options deposited on ceramic samples, we proceeded from the results of previously performed experimental studies on the characteristics of various nitride and DLC coatings performed by the authors of this work [62–64]. Two coating options were selected, such as TiZrN and CrAlSiN/DLC compositions, which demonstrated good tribological properties in contact with materials of various counter bodies. The deposition of a CrAlSiN coating before a DLC coating was caused by the need to reduce internal stresses and improve its adhesion to the ceramic substrate [65–67].

These coating options were formed on  $Al_2O_3/TiC$  and SiAlON ceramics inserts after diamond grinding (initial samples) and after removing the defective layer with beams of fast argon atoms following the technological principles shown in Figure 3.

Table 2 provides information on the technological conditions for the TiZrN and CrAlSiN coatings' deposition on the ceramic samples using magnetron sputtering on the unit shown in Figure 5.



(a)



(b)

**Figure 5.** Experimental technological unit for complex plasma-beam surface treatment of ceramic samples: general view of the unit on the right side (a), and a source of beams of fast atoms of argon mounted on the left side of the unit and its operation principle (b); 1 is a discharge voltage source, 2 is an accelerating voltage source, and 3 is a high-voltage inlet.

**Table 2.** Technological conditions for nitride coating deposition on ceramic samples.

Coating Option	Discharge Current, A	Pressure, Pa	Discharge Voltage, V	Composition of the Gas Mixture, vol. %	Target Composition, wt. %	Deposition Time, min
TiZrN	4.5	0.6	500	40% N <sub>2</sub> ; 60% Ar	TiZr (60% of Ti)	90
CrAlSiN	4.0	0.6	500	40% N <sub>2</sub> ; 60% Ar	AlSi (88% of Al); Cr	65

Deposition of an external DLC coating on the ceramic samples with CrAlSiN coatings was carried out by the gas-phase method in a mixture of acetylene (C<sub>2</sub>H<sub>2</sub>), tetramethylsilane Si(CH<sub>3</sub>)<sub>4</sub>, and argon (Ar). A gas mixture containing 16 vol.% of Si(CH<sub>3</sub>)<sub>4</sub>, 6 vol.% of Ar, and 78 vol.% of N<sub>2</sub> is injected into the vacuum chamber of the unit at 60 min of CrAlSiN coating deposition to form a transition layer between the nitride and DLC coatings. The DLC coating was directly condensed in a vacuum chamber at a temperature of 180 °C in a gas mixture of 3 vol.% of Si(CH<sub>3</sub>)<sub>4</sub>, 52 vol.% of Ar, and 45 vol.% of C<sub>2</sub>H<sub>2</sub> at a pressure of 1.5 Pa and a bias voltage of 500 V. The total deposition time of the DLC coating was 120 min. Figures 6 and 7 show SEM images of fractures of Al<sub>2</sub>O<sub>3</sub>/TiC and SiAlON ceramics samples coated with TiZrN and CrAlSiN/DLC coatings. Table 3 provides information on the main characteristics of coated samples.

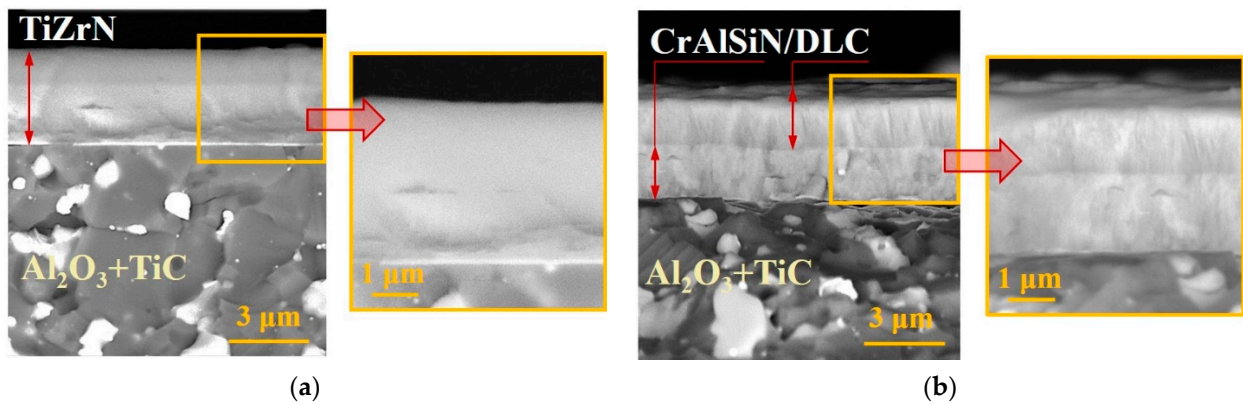


**Figure 6.** SEM images of fractures of Al<sub>2</sub>O<sub>3</sub>/TiC-ceramic samples with two coating options: TiZrN (a) and CrAlSiN/DLC (b).

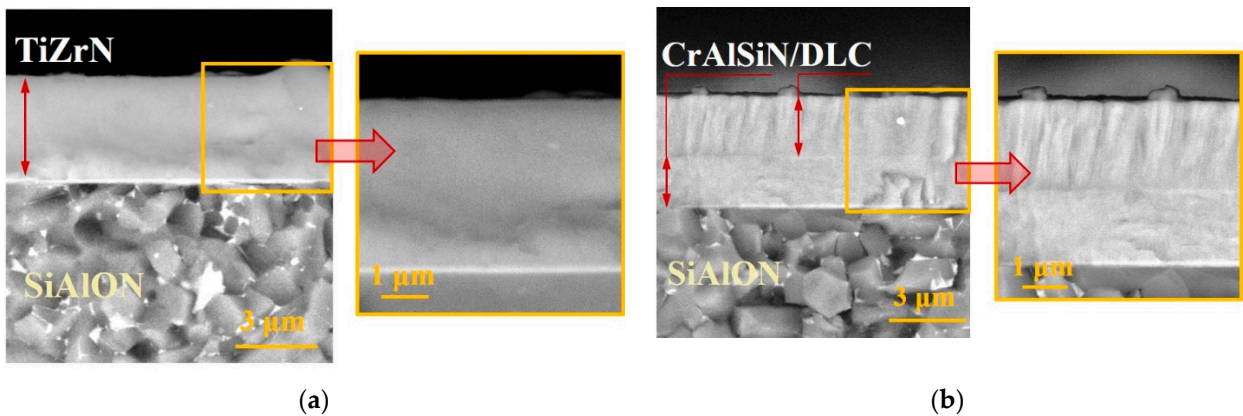


**Figure 7.** SEM images of fractures of SiAlON-ceramic samples with two coating options: TiZrN (a) and CrAlSiN/DLC (b).

**Table 3.** Characteristics of ceramic samples with coatings.

Type of Coatings	Type of Ceramics	Characteristics of Coatings		
		Thickness, $\mu\text{m}$	Martens Hardness, GPa	Average Friction Coefficient at 20 °C
TiZrN	Al <sub>2</sub> O <sub>3</sub> /TiC	3.2	28 ± 1	0.4
	SiAlON	3.2	28 ± 1	0.45
CrAlSiN/DLC	Al <sub>2</sub> O <sub>3</sub> /TiC	3.4	25 ± 2	0.09
	SiAlON	3.5	25 ± 1.5	0.1

Studies of the strength of the adhesive bond of coatings with ceramic samples were carried out on a Nanovea Mechanical Testing M1 device (Nanovea, Irvine, CA, USA) using a scratch testing method with a Rockwell indenter of an increasing load from 1 to 40 N, recording the spectrum of the acoustic emission signal according to the ASTM C1624-05-2015 standard. When conducting tests based on the level of acoustic emission signal, the critical loads of coating destruction and their average values were assessed based on the results of four tests: loads LC<sub>1</sub> and LC<sub>2</sub>, which determine the processes of crack formation and adhesive destruction of the coating, respectively; and load LC<sub>3</sub>, which determines the complete peeling of coatings.

#### 2.5. Study of the Index of Defectiveness and Wear Resistance of Samples Made of Al<sub>2</sub>O<sub>3</sub>/TiC and SiAlON Ceramics

The index of defectiveness criterion and an original method for its calculation, developed by the authors and described in detail in [28], were used to quantify and compare the level of defects in the surface layer of ceramic samples after diamond grinding and after removing the defective layer with beams of fast argon atoms. According to this technique, the index of defectiveness is estimated as the product of the density of defects (total area detected in contrast images) per unit surface area of a ceramic sample and the thickness of the defective layer in the area of the ceramic sample under consideration ( $R_t$  parameter). This technique has already been tested when comparing the states of the surface layer of ceramic inserts after various types of abrasive processing (grinding, finishing, and polishing). It was found that the index of defectiveness is characterized by high sensitivity to minimal changes in the state of the surface layer. Therefore, this criterion was used when conducting research within this work.

Wear-resistance tests on Al<sub>2</sub>O<sub>3</sub>/TiC- and SiAlON-ceramic samples were carried out using two methods simulating abrasive and fretting wear conditions. Figure 8a,b show the schemes and devices for testing the wear resistance of ceramic samples under abrasive and fretting wear. Table 4 shows the conditions for wear-resistance testing Al<sub>2</sub>O<sub>3</sub>/TiC- and SiAlON-ceramic samples.

A Calowear abrasion tester device (CSM Instruments SA, Peseux, Switzerland) was used to assess the wear resistance of the surface layer of ceramic samples to abrasion. During the testing (Figure 8a), an abrasive suspension enters the contact zone between the test sample and the rotating counter body. As a result of contact, a wear spot in the form of a well is formed on the surface of the ceramic sample. Data on the parameters of the well formed on the surface layer of a ceramic sample during abrasive exposure was obtained by contact scanning with a stylus on a Dektak XT profilometer (Bruker AXS, Billerica, MA, USA) [68,69].

A friction machine model 1401 (Moscow Aviation Institute, Moscow, Russia) was used to evaluate the wear resistance of the surface layer of ceramic samples under conditions of small oscillatory and relative displacements (fretting wear) [70,71]. Fretting wear is a typical process of local destruction of a ceramic material that occurs in contact with a counter body under load (Figure 8b). In this case, the contact zone is subject to slight relative movement under the influence of vibration. The ceramic sample performed a reciprocating motion while the counter body remained motionless. As a result of contact, a wear spot in the form

of a well is formed on the surface of the ceramic sample. Investigation of wear spots and measurement of their profiles of the surface layer of the samples was carried out using an Olympus LEXT OLS 5000 confocal microscope (Olympus Corporation, Tokyo, Japan).

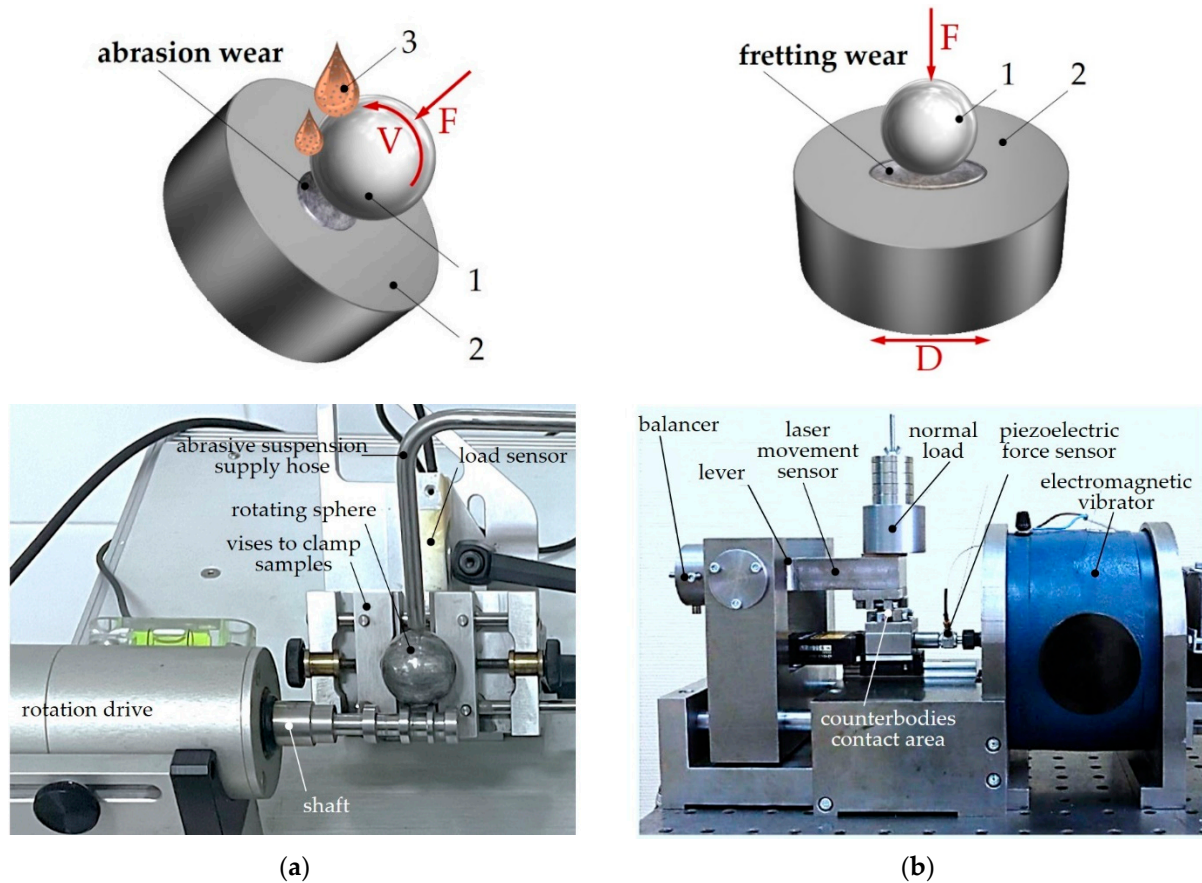


**Figure 8.** Schemes (upper images) and devices (lower images) for testing the wear resistance of samples made of  $Al_2O_3/TiC$  and SiAlON ceramics with coatings under conditions of abrasive (a) and fretting (b) wear, where 1 is a ceramic insert, 2 is a counterbody, and 3 is abrasive suspension.

**Table 4.** Conditions for wear-resistance testing of  $Al_2O_3/TiC$ - and SiAlON-ceramic samples.

Testing Type, Counterbody	Counter Body Rotation Speed, rpm	Contact Force, N	Number of Friction Cycles, Units	Exposure Time, min	Frequency of Movements, Hz	Relative Movement, $\mu m$
Abrasion wear, hardened ball of $\varnothing 20$ mm	950	0.2	-	20	-	-
Fretting wear, hardened ball of $\varnothing 10$ mm	stationary	10	$10^5$	-	100	15

### 3. Results and Discussion

#### 3.1. Influence of Treatment by Beams of Fast Argon Atoms on Surface Layer State of the Samples Made of $Al_2O_3/TiC$ and SiAlON Ceramics

The results of studies on the bombardment of the surface layer of samples made of two ceramics under study with argon atoms with energies in the range of 0.5–7.0 keV show that the energy parameter is the key one. Its change significantly affects the sputtering coefficient, which is determined by the ratio of the number of emitted atoms to the number of atoms bombarding the surface layer (Figure 9a).

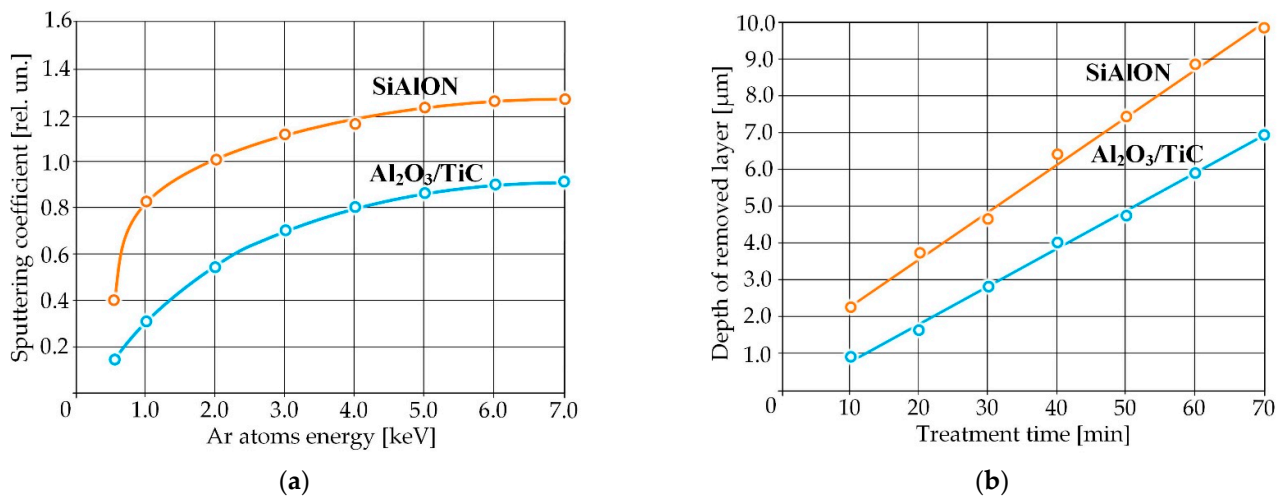


**Figure 9.** Dependences of sputtering coefficients on the energy of Ar atoms bombarding the surface layer (a) and the depth of the removed layer (b) on the treatment time for Al<sub>2</sub>O<sub>3</sub>/TiC and SiAlON ceramics.

It has been established that the sputtering coefficient of Al<sub>2</sub>O<sub>3</sub>/TiC and SiAlON ceramics tends to increase as the particle energy increases to a value of ~5 keV. With a further increase in energy, the growth of the sputtering coefficient slows down. The latter circumstance is associated with increased energy losses for heating the ceramic samples under processing [72]. Therefore, the energy of argon atoms bombarding the surface layer of ceramic samples for implementing the technological principles of surface treatment proposed in the research was 5 keV.

It has been experimentally established (Figure 9b) that the dependence of the etching depth by argon particles with energies of 5 keV on the treatment time for the two ceramics under study is generally linear. However, the etching rate (removal of the defective layer) differs significantly and amounts to 5.9–6.0 μm/h for Al<sub>2</sub>O<sub>3</sub>/TiC and 8.8–8.9 μm/h for SiAlON. The roughness of the surface of the samples after treatment in terms of the R<sub>a</sub> parameter, also assessed during the experiments, changed slightly with increasing treatment time and varied at 0.14–0.16 μm for Al<sub>2</sub>O<sub>3</sub>/TiC and 0.12–0.14 μm for SiAlON over 70 min of exposure. The rational time of exposure of argon particles is 70 min for Al<sub>2</sub>O<sub>3</sub>/TiC and 48 min for SiAlON to ensure guaranteed removal of the surface defective layer formed during diamond grinding and to achieve an etching depth of about 7.0 μm.

Figures 10 and 11 show comparative results of studies of microstructures and profilograms of the surface layer of the same samples of inserts made of Al<sub>2</sub>O<sub>3</sub>/TiC and SiAlON ceramics after diamond grinding and after treatment with argon atoms with energies of 5 keV during 70 and 48 min, respectively.

The microstructures and profilograms of ceramic samples after bombardment with beams of argon atoms clearly show a transformation of the surface layer, accompanied by the removal of numerous defects present in large numbers on the original samples subjected to diamond grinding (Figures 10 and 11).

In addition to the pronounced visual differences, the results of a quantitative assessment of various indicators of the state of the surface layer (Table 5) testify even more convincingly about the changes that occurred after treatment with beams of accelerated argon atoms. The given average values of the index of defectiveness of ceramic samples are calculated based on the results measurements of 10 inserts of each type of ceramic under study. Table 5 also provides data on the parameters of the surface layer of the samples achieved through diamond grinding and polishing to compare them.

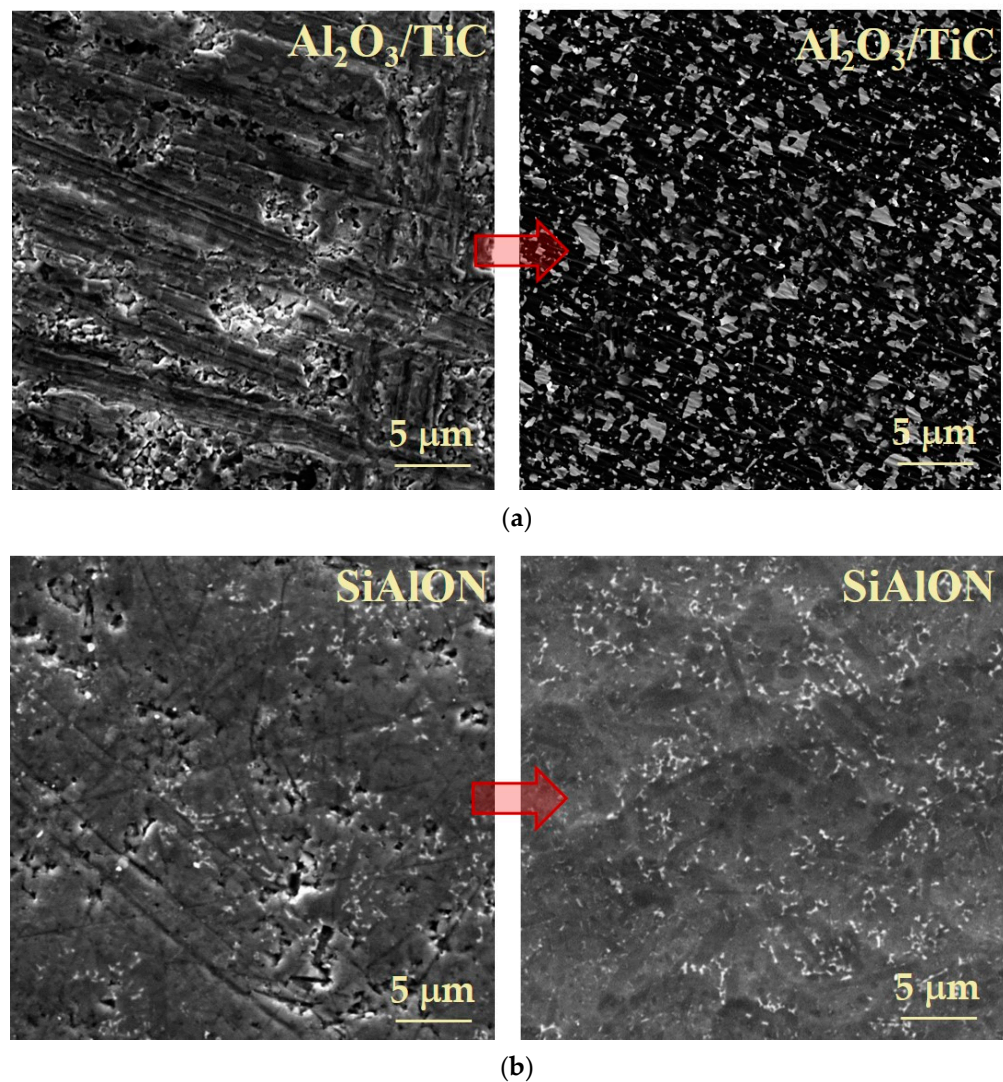


**Figure 10.** SEM images of the microstructure of the surface layer of samples made of  $\text{Al}_2\text{O}_3/\text{TiC}$  (a) and SiAlON ceramics (b) after diamond grinding (left) and bombardment with argon atoms (right).

**Table 5.** Indicators of the state of the surface layer of samples made of  $\text{Al}_2\text{O}_3/\text{TiC}$  and SiAlON ceramics after various types of processing.

Types of Ceramics	Types of Processing	Indicators of the Surface Layer Condition			
		Density of Defects $\rho$	Max Depth of Defective Layer $R_t, \mu\text{m}$	Index of Defectiveness $\rho \cdot R_t, \mu\text{m}$	Roughness Parameter $R_a, \mu\text{m}$
$\text{Al}_2\text{O}_3/\text{TiC}$	Diamond grinding	0.4	4.17	1.67	0.31
	Treatment with argon atoms with an energy of 5 keV for 70 min	0.012	0.46	0.0055	0.16
	Diamond grinding, finishing, and polishing	0.005	0.4	0.002	0.002
SiAlON	Diamond grinding	0.33	3.27	1.08	0.29
	Treatment with argon atoms with an energy of 5 keV for 48 min	0.01	0.46	0.0046	0.14
	Diamond grinding, finishing, and polishing	0.004	0.38	0.0015	0.0014

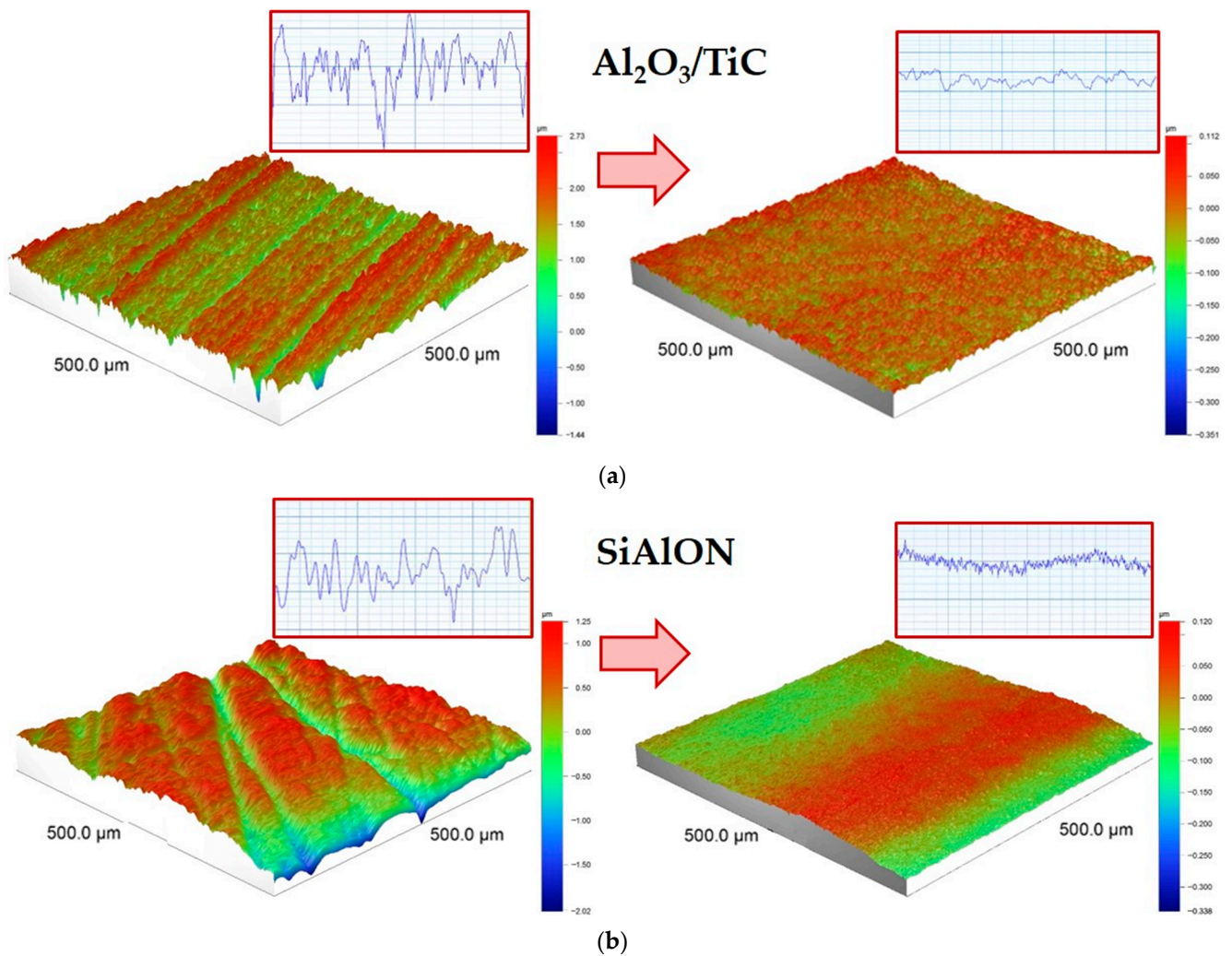


**Figure 11.** Profilograms of the surface layer of samples made of  $\text{Al}_2\text{O}_3/\text{TiC}$  (a) and  $\text{SiAlON}$  ceramics (b) after diamond grinding (left) and bombardment with argon atoms (right).

The experimental data presented show that the proposed technological approach, which involves etching with argon atoms, ensures almost complete removal of the defective layer (from 4.17 to 0.46  $\mu\text{m}$  for  $\text{Al}_2\text{O}_3/\text{TiC}$  and from 3.27 to 0.46  $\mu\text{m}$  for  $\text{SiAlON}$ ) and greatly reduces the index of defectiveness comparing to the value achieved by traditional diamond grinding. Those results for samples made of  $\text{Al}_2\text{O}_3/\text{TiC}$  and  $\text{SiAlON}$  ceramics should be considered extremely significant, considering the high productivity and manufacturability of the proposed approach and the absence of the need to use expensive equipment even compared with the index of defectiveness for the surface layer achieved by diamond polishing the etching with argon atoms provides slightly higher values of this indicator.

In addition, the experiments confirmed the significant influence of the state of the surface layer of ceramic samples on the quality of subsequently deposited coatings (in the case of the two compositions under study, namely  $\text{TiZrN}$  and  $\text{CrAlSiN/DLC}$ ). As is seen in the SEM images (Figure 12), the increased density of defects in the surface layer of ceramic samples formed during diamond grinding indicates that its microstructure is characterized by a high degree of heterogeneity and porosity. It can be assumed that this is a consequence of the misorientation of the grains of the deposited film and the deterioration of growth conditions of the coating, which was observed by the authors of [73–75] that deposited various coatings on substrates with an increased level of microroughness.

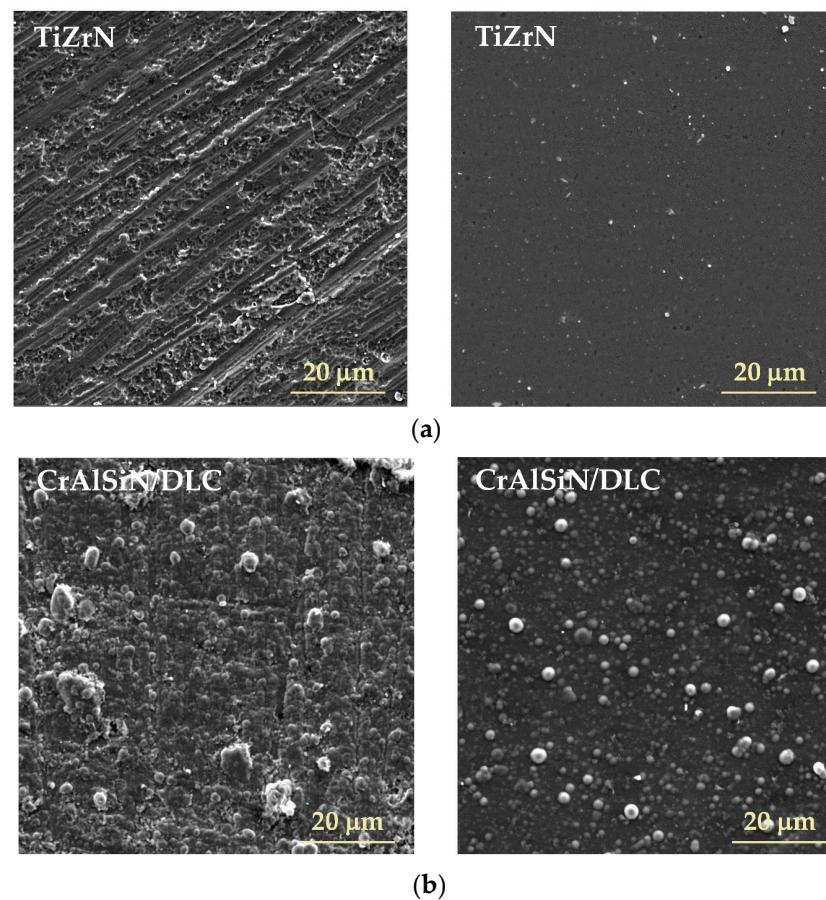


**Figure 12.** SEM images of the microstructure of the surface layer of TiZrN (a) and CrAlSiN/DLC (b) coatings deposited on samples made of  $\text{Al}_2\text{O}_3/\text{TiC}$  ceramics after diamond grinding (left) and after removing the defective layer by bombardment with argon atoms (right).

At the same time, the defects associated with the state of the ceramic substrate are not observed in the microstructure of the coating formed on a ceramic sample with the previously removed by bombardment with argon atoms defective layer. The effect was observed for both TiZrN and CrAlSiN/DLC coatings. The observation correlates with the results of other works [76,77]. It allows us to conclude that the highly defective surface layer of ceramic samples predetermines the formation of defective coatings, which will not be able to fully perform their functions aimed at increasing the wear resistance of contact surfaces of a ceramic product under increased mechanical loads.

### 3.2. Wear Resistance of Samples Made of $\text{Al}_2\text{O}_3/\text{TiC}$ and SiAlON Ceramics after Complex Plasma-Beam Surface Treatment under Conditions of Abrasive Wear

The testing carried out under conditions of abrasive exposure on the surface layer of ceramic inserts showed that a wear spot in the form of a spherical well is formed on the surface of the samples due to contact with the counter body and abrasive particles. Qualitative and quantitative assessments of volumetric wear provide clues to the following:

- The resistance to abrasive wear of ceramic samples;
- The effectiveness of various coatings;
- The contribution to the wear resistance of the state of the surface layer on which the coatings are deposited.

Figures 13 and 14 show typical wear wells after testing samples of  $\text{Al}_2\text{O}_3/\text{TiC}$  and SiAlON ceramics with TiZrN and CrAlSiN/DLC coatings deposited on a defective surface layer (after diamond grinding) and after removing the layer by bombardment with argon atoms. The kinetics of the development of wear spots over time of abrasive exposure

on ceramic samples with coatings is presented in Figure 15. The experimental results demonstrate that the deposition of coatings of two selected compositions significantly reduces the wear rate of  $\text{Al}_2\text{O}_3/\text{TiC}$ - and  $\text{SiAlON}$ -ceramic samples under conditions of abrasive exposure. As seen from the experimental data (Figures 14 and 15), the state of the ceramic base, characterized by the index of defectiveness (Table 5), significantly affects the wear resistance of subsequently deposited coatings for  $\text{Al}_2\text{O}_3/\text{TiC}$  and  $\text{SiAlON}$  ceramics. For example, during the testing of some samples with coatings deposited on defective ceramic inserts, their peeling was observed when an external load was applied (this was observed in samples with  $\text{TiZrN}$  coatings; Figure 13). The insufficient efficiency of the coatings is well explained by SEM images of their surface, which contain numerous microstructural defects (Figure 12). Discontinuous and porous coatings formed on a ceramic base are characterized by low adhesive bond strength [78], which inevitably leads to their local delamination under mechanical loads. This is confirmed by the experimentally obtained results of assessing the strength of the adhesive bond of  $\text{TiZrN}$  and  $\text{CrAlSiN/DLC}$  coatings with  $\text{Al}_2\text{O}_3/\text{TiC}$ - and  $\text{SiAlON}$ -ceramic samples (Table 6). It can be seen that cracking in coatings containing numerous pores and discontinuities occurs at relatively small loads  $\text{LC}_1$ , which are approximately 40–50% less than the corresponding loads recorded for defect-free samples. Adhesive failure ( $\text{LC}_2$ ) and complete peeling ( $\text{LC}_3$ ) of porous coatings are observed at loads approximately 20–30% lower. Such coatings are incapable of ensuring a stable, anti-friction, wear-resistant film at the “counter body–coating” interface. It should be emphasized that a certain decrease in the wear rate of the original ceramic samples is observed even in the presence of  $\text{TiZrN}$  and  $\text{CrAlSiN/DLC}$  coatings on ceramic inserts, which have microstructural defects. It is associated with ongoing changes in the conditions of frictional interaction with the counter body. However, such coatings are noticeably inferior in efficiency throughout the entire testing to the same coatings deposited on samples with a previously removed defective layer and have a many times lower index of defectiveness (Figure 15).

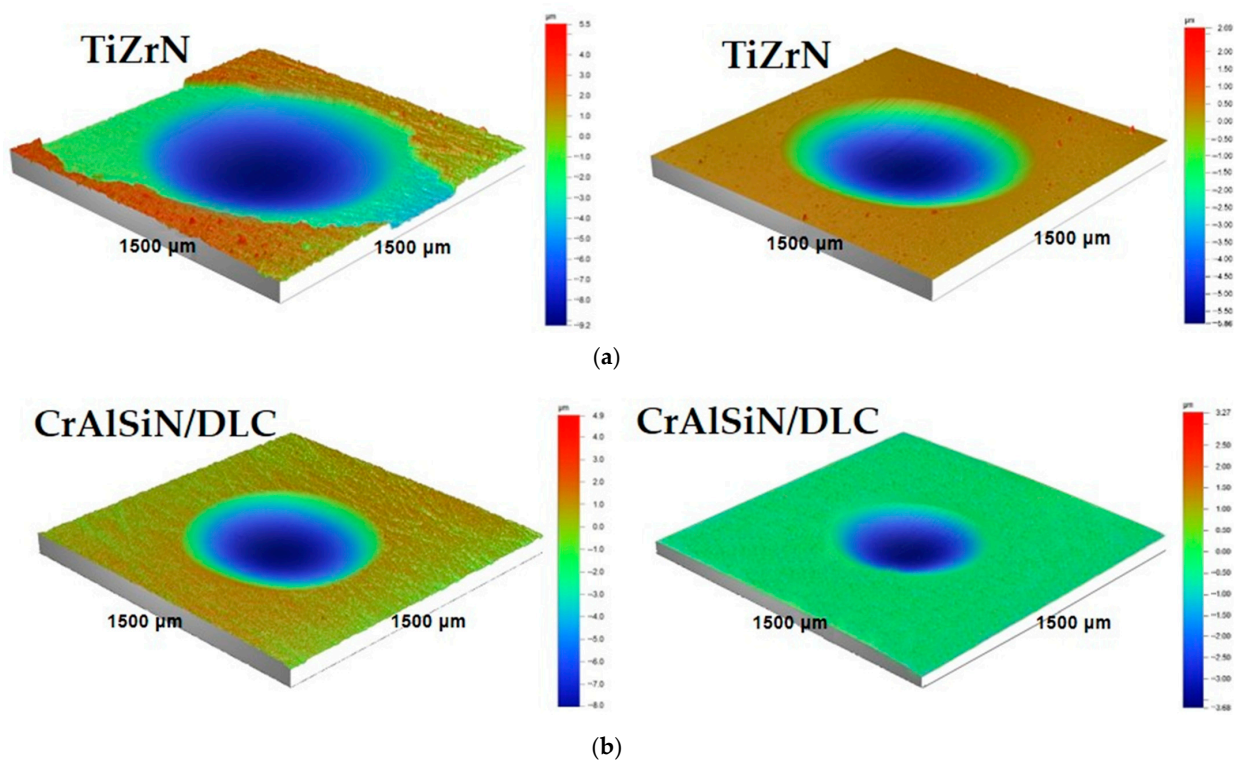


**Figure 13.** Profilograms of wear spots after 20 min of abrasive exposure on samples made of  $\text{Al}_2\text{O}_3/\text{TiC}$  ceramics with coatings deposited on the surface layer after diamond grinding (left) and bombardment with argon atoms (right): (a)  $\text{TiZrN}$  coating and (b)  $\text{CrAlSiN/DLC}$  coating.

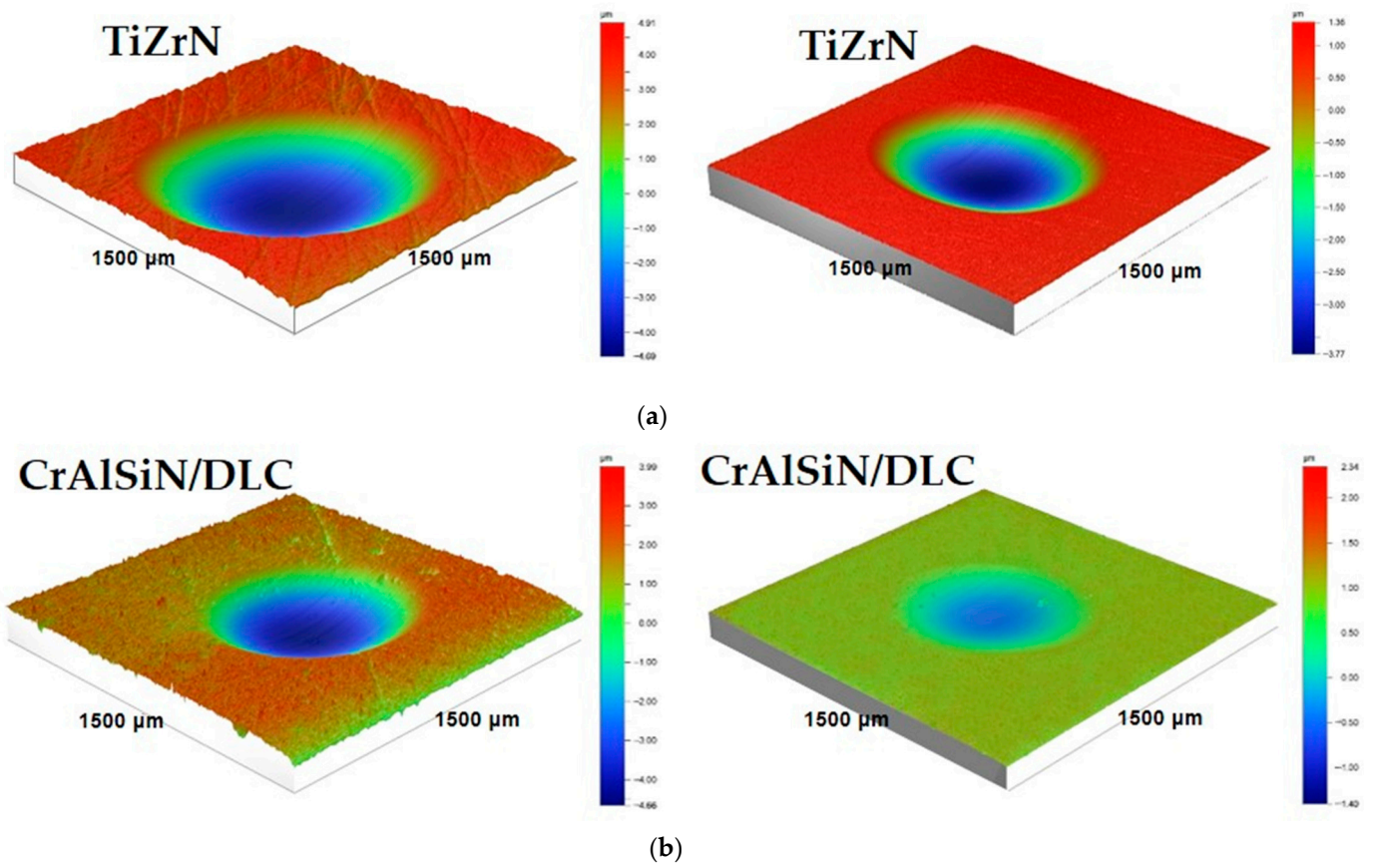


**Figure 14.** Profilograms of wear spots after 20 min of abrasive exposure on samples made of SiAlON ceramics with coatings deposited on the surface layer after diamond grinding (left) and bombardment with argon atoms (right): (a) TiZrN coating and (b) CrAlSiN/DLC coating.

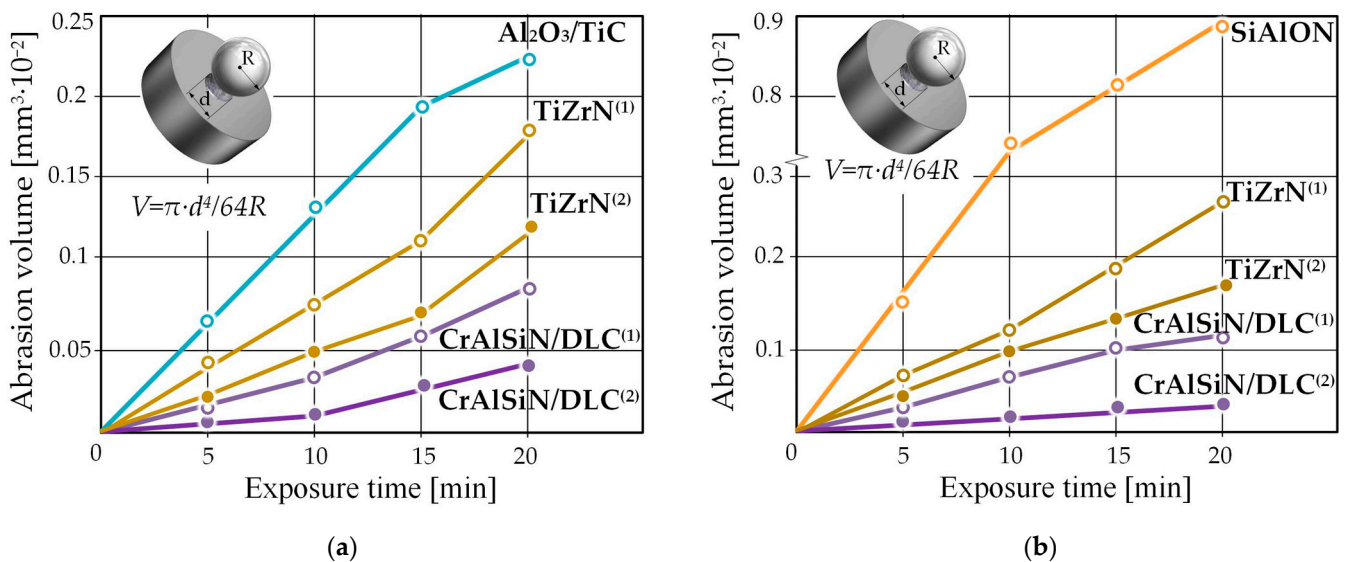


**Figure 15.** Kinetics of development of wear spots over time of abrasive exposure on ceramic samples made of Al<sub>2</sub>O<sub>3</sub>/TiC (a) and SiAlON (b) ceramics with coatings deposited after diamond grinding (1) and bombardment with argon atoms (2).

**Table 6.** Strength of the adhesion bond of TiZrN and CrAlSiN/DLC coatings deposited on samples of Al<sub>2</sub>O<sub>3</sub>/TiC- and SiAlON-ceramics with different states of the surface layer.

Types of Ceramics	Types of Processing	Coating Composition	Average Critical Load Value, N		
			LC <sub>1</sub>	LC <sub>2</sub>	LC <sub>3</sub>
Al <sub>2</sub> O <sub>3</sub> /TiC	Diamond grinding	TiZrN	16 ± 2	23 ± 4	29 ± 3
		CrAlSiN/DLC	18 ± 3	23 ± 2	30 ± 2
	Treatment with argon atoms with an energy of 5 keV for 70 min	TiZrN	24 ± 3	28 ± 2	36 ± 3
		CrAlSiN/DLC	25 ± 1	31 ± 1	37 ± 2
SiAlON	Diamond grinding	TiZrN	15 ± 3	21 ± 2	28 ± 3
		CrAlSiN/DLC	17 ± 2	22 ± 3	29 ± 2
	Treatment with argon atoms with an energy of 5 keV for 48 min	TiZrN	23 ± 2	27 ± 2	34 ± 2
		CrAlSiN/DLC	24 ± 3	29 ± 3	37 ± 1

Additional confirmation of the conclusion made about the change in the conditions of frictional interaction with the counter body for the same coatings, but deposited on ceramic samples made of Al<sub>2</sub>O<sub>3</sub>/TiC with different states of the surface layer, are the experimental results of estimating the friction coefficient shown in Figure 16 (data obtained under friction conditions—sliding under a load of 10 N with a speed of 0.1 m/s when using counter bodies in the shape of a hardened steel ball with a diameter of 6 mm). For coatings deposited on ceramic samples after removing the defective layer (right images in Figure 16), the coating and counter body are worn in at the initial moment of testing, after which the friction coefficient stabilizes and has a monotonic character throughout the entire testing time with a value of 0.4–0.45 for the TiZrN coating and 0.09 for the CrAlSiN/DLC coating. The friction coefficient change curves for the same coatings deposited on ceramic samples after diamond grinding (left images in Figure 16) have a fundamentally different character. It can be seen that the friction coefficient changes abruptly, and the friction conditions are unstable. This nature of the friction coefficient curves, apparently, results from alternating processes of adhesion of contacting surfaces and destruction of “bridges” of adhesive bonds. The above indirectly indicates the absence of a strong boundary film and more intense adhesion in the tribocontact zone when contacting partial and porous TiZrN and CrAlSiN/DLC coatings, which are deposited on ceramic substrates after diamond grinding.

In quantitative terms, the differences in the wear resistance of coatings deposited on ceramics with different surface layer states are as follows. The volumetric wear during abrasive wear of the original Al<sub>2</sub>O<sub>3</sub>/TiC-ceramic samples decreases by 1.2 times when TiZrN coatings are deposited after diamond grinding and by 1.9 times when those coatings are deposited after removing the defective layer. The volumetric wear of those ceramics reduces by 2.8 and 5.7 times, respectively, when depositing the CrAlSiN/DLC coatings (Figure 15a). For the original SiAlON-ceramic samples, the volumetric wear decreases by 3.1 times when TiZrN coatings are deposited after diamond grinding and by 5 times when those coatings are deposited after removing the defective layer. The volumetric wear of those ceramics reduces by 8.1 and 22.5 times, respectively, when depositing CrAlSiN/DLC coatings (Figure 15b).

At the same time, the coating effect is most pronounced for SiAlON ceramics. Under the same testing conditions, the original SiAlON-ceramic samples have noticeably greater volumetric wear than Al<sub>2</sub>O<sub>3</sub>/TiC-ceramic samples. The effect is due to the higher hardness of Al<sub>2</sub>O<sub>3</sub>/TiC (Table 1) and the fact that this indicator primarily determines the resistance to abrasive wear [79]. In addition, Al<sub>2</sub>O<sub>3</sub>/TiC ceramics are characterized by a slightly lower coefficient of friction against steel compared to SiAlON ceramics, which also affects the wear rate when interacting with the counter body [80,81].

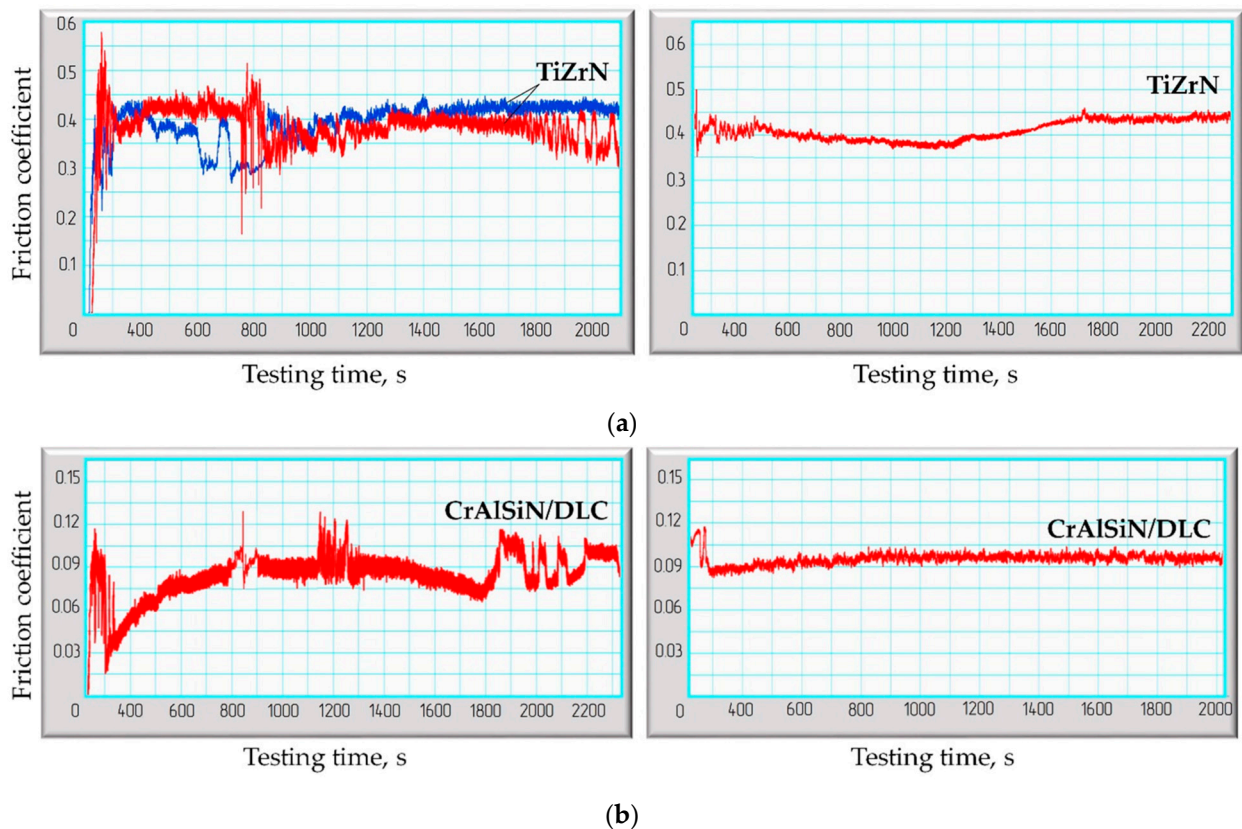


**Figure 16.** The nature of the change over time in the friction coefficient of samples made of  $\text{Al}_2\text{O}_3/\text{TiC}$  ceramics with TiZrN (a) and CrAlSiN/DLC (b) coatings deposited on the surface layer after diamond grinding (left) and bombardment with argon atoms (right).

### 3.3. Wear Resistance of Samples Made of $\text{Al}_2\text{O}_3/\text{TiC}$ and SiAlON Ceramics after Complex Plasma-Beam Surface Treatment under Conditions of Fretting Wear

Figures 17 and 18 show optical images of wear spots on samples of  $\text{Al}_2\text{O}_3/\text{TiC}$  and SiAlON ceramics formed during testing under fretting conditions (after 105 friction cycles). Experimental results are presented for ceramic samples with TiZrN and CrAlSiN/DLC coatings deposited to the surface layer after various types of processing, such as diamond grinding and bombardment with argon atoms with energy of 5 keV. It was found that, as in the case of abrasive wear, the state of the surface layer (its defectiveness) also significantly contributes to the wear rate of samples made of  $\text{Al}_2\text{O}_3/\text{TiC}$  and SiAlON ceramics under conditions of fretting wear. At the wear spots (Figures 17 and 18), qualitative differences are brightly pronounced in the area of tribocontact of ceramic samples with different defects in the surface layer. It can be seen that the two variants of the coatings deposited on ceramic samples after diamond grinding are characterized by significantly larger sizes of wear spots and by the significant adhesion of particles detached from the materials during testing (wear products). It is apparently due to the already discussed discontinuity of coatings formed on ceramic samples after diamond grinding, their probable local delamination under mechanical loads, and the absence of a stable boundary anti-friction film between the ceramics and the counter body. The normal force has fairly large values, and the slippage amplitude is very small, which makes it difficult to remove wear products from the tribocontact zone and promotes their adhesion to the ceramics, which can further accelerate wear under fretting conditions. The coating performs anti-friction and protective functions for a longer time and minimizes the amount of wear products in the case of its deposition on a ceramic base after removing the defective layer. Such coatings on the contact surfaces of ceramic samples constrain the development of a wear spot and reduce the size of those spots compared to samples with discontinuous and porous coatings.

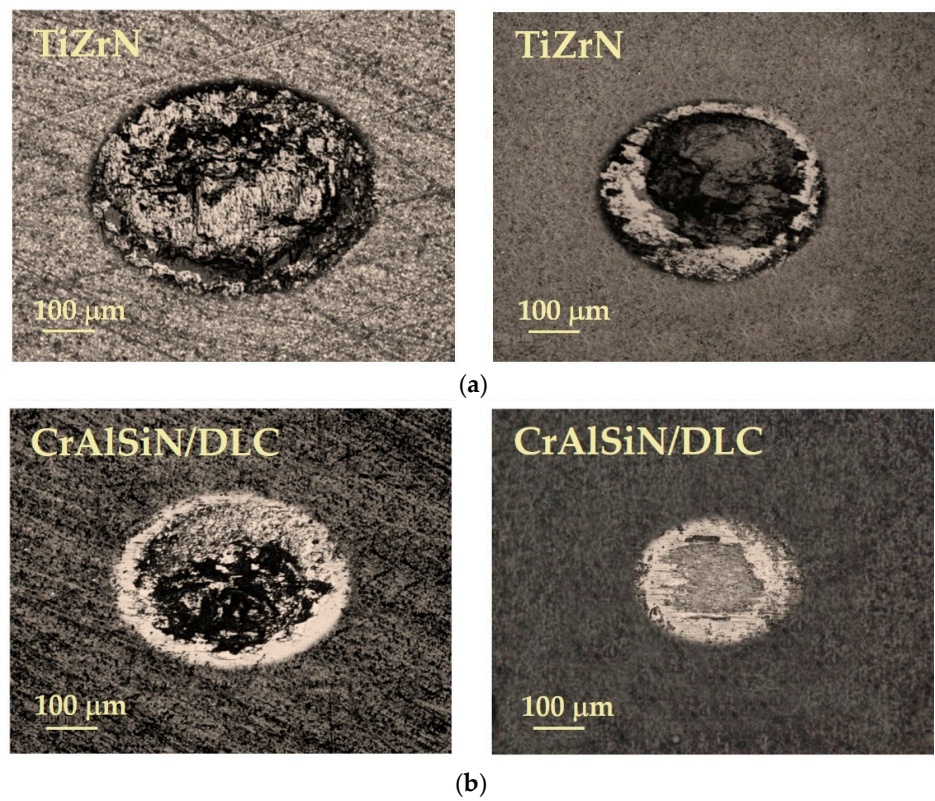


**Figure 17.** Wear spots after 105 cycles of friction of counter bodies with samples made of  $\text{Al}_2\text{O}_3/\text{TiC}$  ceramics with coatings deposited on the surface layer after diamond grinding (left) and bombardment with argon atoms (right): (a) TiZrN coating and (b) CrAlSiN/DLC coating.

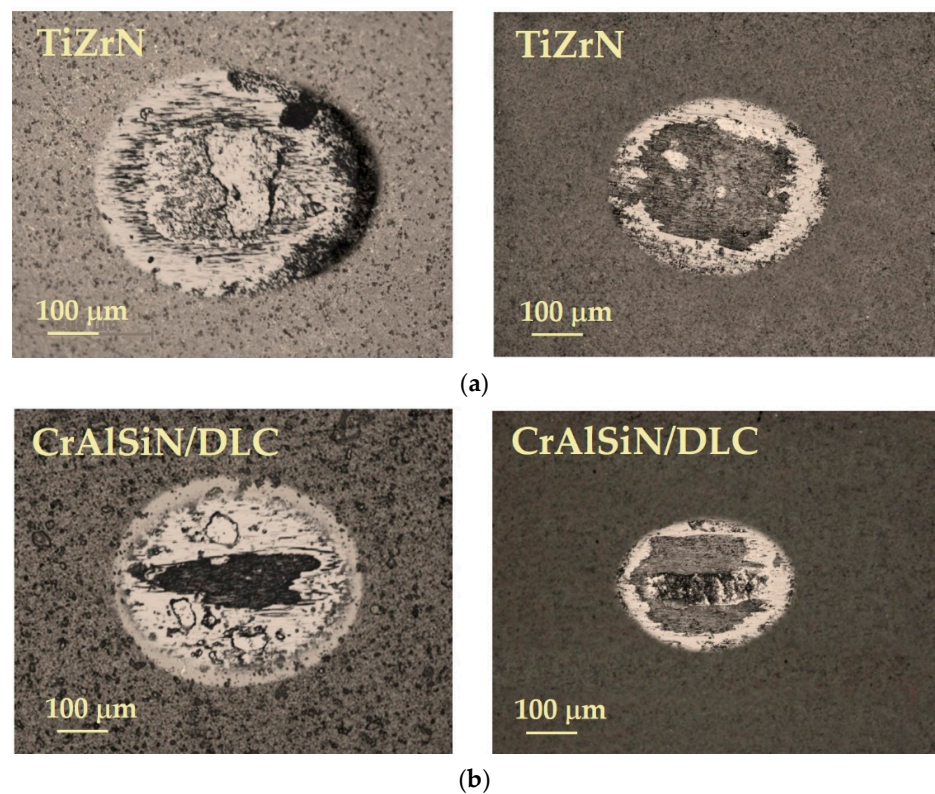


**Figure 18.** Wear spots after 105 cycles of friction of counter bodies with samples made of SiAlON ceramics with coatings deposited on the surface layer after diamond grinding (left) and bombardment with argon atoms (right): (a) TiZrN coating and (b) CrAlSiN/DLC coating.

A quantitative assessment of the wear resistance of coatings deposited on ceramic samples with different states of the surface layer after testing under fretting conditions is presented in Figure 19. The volumetric wear during testing under fretting conditions for original  $\text{Al}_2\text{O}_3/\text{TiC}$ -ceramic samples decreases by 1.4 times when TiZrN coatings are deposited after diamond grinding and by 2.0 times after removing the defective layer. The volumetric wear of those ceramics reduces by 1.5 and 3.1 times, respectively, when depositing the CrAlSiN/DLC coatings (Figure 19a). For the original SiAlON-ceramic samples, the volumetric wear decreases by 1.4 times when TiZrN coatings are deposited after diamond grinding and by 2.5 times after removing the defective layer. The volumetric wear of those ceramics reduces by 1.7 and 4.0 times, respectively, when depositing CrAlSiN/DLC coatings (Figure 19b).

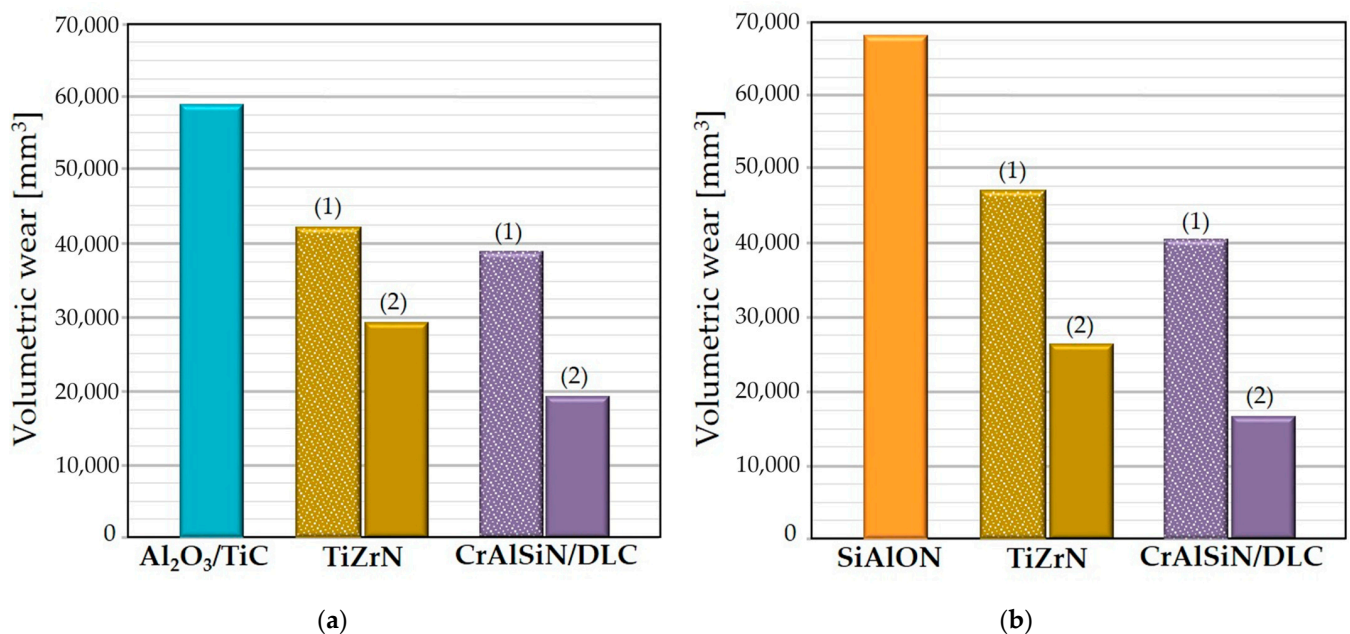


**Figure 19.** Volumetric wear after fretting wear testing of ceramic samples made of  $\text{Al}_2\text{O}_3/\text{TiC}$  (a) and SiAlON (b) with coatings deposited after diamond grinding (1) and bombardment with argon atoms (2).

#### 4. Conclusions

- (1) Intense thermomechanical action during high-performance diamond grinding during the shaping of sintered ceramic blanks (for example,  $\text{Al}_2\text{O}_3/\text{TiC}$  and SiAlON), as a result of which the required allowance is removed, leads to the formation of a surface layer with numerous defects.
- (2) Increased defectiveness of the surface layer of ceramic samples after diamond grinding when depositing functional coatings (for example, TiZrN and CrAlSiN/DLC) significantly worsens the conditions for the film growth and predetermines the formation of discontinuous and porous coatings that cannot ensure a stable anti-friction wear-resistant film at the “counter body–coating” interface, which reduces the potential effectiveness of coatings under conditions of abrasive exposure and fretting wear.
- (3) The equipment and technological approach described by the authors and based on “dry” etching (bombardment) of the surface with beams of accelerated argon particles, which occurs with physical sputtering of the surface layer to the required depth, can be used for high-performance removal of defects from the surface of ceramic samples after diamond grinding (the etching rates of 5.9–6.0  $\mu\text{m}/\text{h}$  for  $\text{Al}_2\text{O}_3/\text{TiC}$  and 8.8–8.9  $\mu\text{m}/\text{h}$  for SiAlON).
- (4) The proposed technological approach, involving etching with argon atoms with an energy of 5 keV, ensures almost complete removal of the defective layer on samples

made of Al<sub>2</sub>O<sub>3</sub>/TiC and SiAlON ceramics and reduces the index of defectiveness of the surface layer, calculated as the product of density of defects per unit surface area and the defective layer's thickness, by several orders of magnitude comparing that indicator for traditional diamond grinding.

- (5) There are no pronounced discontinuities and pores in the microstructure of TiZrN and CrAlSiN/DLC coatings deposited on a “defect-free” surface layer. Under mechanical loads, those coatings ensure a stable boundary anti-friction film between the ceramic material and the counter body. That significantly increases the wear resistance of Al<sub>2</sub>O<sub>3</sub>/TiC- and SiAlON-ceramic samples.
- (6) Complex plasma-beam surface treatment of ceramic samples, including removal of the defective layer and subsequent deposition of functional coatings, provides a reduction in volumetric wear of Al<sub>2</sub>O<sub>3</sub>/TiC ceramics after diamond grinding by 1.9 times for TiZrN coatings and by 5.7 times for CrAlSiN/DLC coatings under conditions of abrasive wear (at 20 min exposure). The volumetric wear of SiAlON ceramics after diamond grinding is reduced by 5 times for TiZrN coatings and by 22.5 times for CrAlSiN/DLC coatings.
- (7) Complex plasma-beam surface treatment of ceramic samples provides a reduction in volumetric wear of Al<sub>2</sub>O<sub>3</sub>/TiC ceramics after diamond grinding by 2.0 times for TiZrN coatings and by 3.1 times for CrAlSiN/DLC coatings under conditions of fretting wear (at 105 friction cycles). The volumetric wear of SiAlON ceramics after diamond grinding is reduced by 2.5 times for TiZrN coatings and by 4.0 times for CrAlSiN/DLC coatings.

**Author Contributions:** Conceptualization, M.A.V.; methodology, M.A.V. and S.N.G.; software, M.A.L. and A.P.M.; validation, M.A.L. and A.P.M.; formal analysis, A.A.O. and N.V.K.; investigation, M.A.L. and A.P.M.; resources, S.N.G.; data curation, A.A.O. and N.V.K.; writing—original draft preparation, M.A.V.; writing—review and editing, M.A.V.; visualization, M.A.V.; supervision, S.N.G.; project administration, M.A.V.; funding acquisition, M.A.V. and S.N.G. All authors have read and agreed to the published version of the manuscript.

**Funding:** This work was funded by the state assignment of the Ministry of Science and Higher Education of the Russian Federation, Project No. FSFS-2023-0003.

**Data Availability Statement:** Data are contained within the article.

**Acknowledgments:** This study was carried out on the equipment of the Center of Collective Use “State Engineering Center” of MSUT “STANKIN” supported by the Ministry of Higher Education of the Russian Federation (project 075-15-2021-695 from 26 July 2021, unique identifier RF 2296.61321X0013).

**Conflicts of Interest:** The authors declare no conflict of interest.

## References

1. Wang, Z.; Liu, Y.; Zou, B.; Huang, C.Z.; Xue, K.; Shi, Z.Y. Mechanical properties and microstructure of Al<sub>2</sub>O<sub>3</sub>-SiCw ceramic tool material toughened by Si<sub>3</sub>N<sub>4</sub> particles. *Ceram. Int.* **2019**, *46*, 8845–8852. [[CrossRef](#)]
2. Zhai, W.; Bai, L.; Zhou, R.; Fan, X.; Kang, G.; Liu, Y.; Zhou, K. Recent Progress on Wear-Resistant Materials: Designs, Properties, and Applications. *Adv. Sci.* **2021**, *8*, 2003739. [[CrossRef](#)]
3. Shi, F. (Ed.) *Ceramic Materials—Progress in Modern Ceramics*; InTech: London, UK, 2012; 242p. [[CrossRef](#)]
4. Ming, W.; Jiang, Z.; Luo, G.; Xu, Y.; He, W.; Xie, Z.; Shen, D.; Li, L. Progress in Transparent Nano-Ceramics and Their Potential Applications. *Nanomaterials* **2022**, *12*, 1491. [[CrossRef](#)]
5. Fedorov, S.; Swe, M.H.; Kapitanov, A.; Egorov, S. Wear of carbide inserts with complex surface treatment when milling nickel alloy. *Mech. Ind.* **2017**, *18*, 710. [[CrossRef](#)]
6. Skela, B.; Sedlaček, M.; Kafexhiu, F.; Podgornik, B. Influence of Microstructure and Mechanical Properties of Hot-work Tool Steel on Wear Resistance Subjected to High-stress Wear Conditions. *Tribol. Lett.* **2020**, *68*, 58. [[CrossRef](#)]
7. Sedlaček, M.; Klančnik, G.; Nagode, A.; Burja, J. Influence of Austempering of As-Cast Medium Carbon High-Silicon Steel on Wear Resistance. *Materials* **2021**, *14*, 7518. [[CrossRef](#)]
8. Wei, S.Z.; Xu, L.J. Review on research progress of steel and iron wear-resistant materials. *Acta Metall. Sin.* **2020**, *56*, 523–538.

9. Rizzo, A.; Goel, S.; Luisa Grilli, M.; Iglesias, R.; Jaworska, L.; Lapkovskis, V.; Novak, P.; Postolnyi, B.O.; Valerini, D. The Critical Raw Materials in Cutting Tools for Machining Applications: A Review. *Materials* **2020**, *13*, 1377. [[CrossRef](#)]
10. Bobzin, K. High-performance coatings for cutting tools. *CIRP J. Manuf. Sci. Technol.* **2017**, *18*, 1–9. [[CrossRef](#)]
11. Mamalis, A.G.; Kundrak, J.; Gyani, K.; Horvath, M. On the Precision Grinding of Advanced Ceramics. *Int. J. Adv. Manuf. Technol.* **2002**, *20*, 255–258.
12. Fedorov, S.V.; Ostrikov, E.A.; Mustafaev, E.S.; Hamdy, K. The formation of the cutting tool microgeometry by pulsed laser ablation. *Mech. Ind.* **2019**, *19*, 703. [[CrossRef](#)]
13. Ruggles-Wrenn, M.B.; Lanser, R.L. Tension-compression fatigue of an oxide/oxide ceramic composite at elevated temperature. *Mater. Sci. Eng. A* **2016**, *659*, 270–277. [[CrossRef](#)]
14. Evans, A.G. Design and life prediction issues for high-temperature engineering ceramics and their composites. *Acta Mater.* **1997**, *45*, 23–40. [[CrossRef](#)]
15. Kuzin, V.V.; Grigor'ev, S.N.; Volosova, M.A. Effect of a TiC Coating on the Stress-Strain State of a Plate of a High-Density Nitride Ceramic Under Nonsteady Thermoelastic Conditions. *Refract. Ind. Ceram.* **2014**, *54*, 376–380. [[CrossRef](#)]
16. Hsu, S.M.; Shen, M. Wear prediction of ceramics. *Wear* **2004**, *256*, 867–878. [[CrossRef](#)]
17. Fedorov, S.V.; Aleshin, S.V.; Swe, M.H.; Abdirova, R.D.; Kapitanov, A.V.; Egorov, S.B. Comprehensive surface treatment of high-speed steel tool. *Mech. Ind.* **2017**, *18*, 2017066. [[CrossRef](#)]
18. Zhang, D.; Li, C.; Jia, D.; Zhang, Y. Investigation into Engineering Ceramics Grinding Mechanism and the Influential Factors of the Grinding Force. *Int. J. Control Autom.* **2014**, *7*, 19–34. [[CrossRef](#)]
19. Zhao, B.; Liu, H.; Huang, C.; Wang, J.; Cheng, M. Fabrication and mechanical properties of Al<sub>2</sub>O<sub>3</sub>-SiCw-TiCnp ceramic tool material. *Ceram. Int.* **2017**, *43*, 10224–10230. [[CrossRef](#)]
20. Lukianova, O.A.; Novikov, V.Y.; Parkhomenko, A.A.; Sirota, V.V.; Krasilnikov, V.V. Microstructure of spark plasma-sintered silicon nitride ceramics. *Nanoscale Res. Lett.* **2017**, *12*, 293. [[CrossRef](#)]
21. Uhlmann, E.; Hübert, C. Tool grinding of end mill cutting tools made from high performance ceramics and cemented carbides. *CIRP Ann.* **2011**, *60*, 359–362. [[CrossRef](#)]
22. Arai, S.A.; Wilson, S.A.; Corbett, J.; Whatmore, R.W. Ultra-precision grinding of PZT ceramics—Surface integrity control and tooling design. *Int. J. Mach. Tools Manuf.* **2009**, *49*, 998–1007. [[CrossRef](#)]
23. Kacalak, W.; Lipiński, D.; Szafraniec, F.; Bałasz, B. A Method and Device for Automated Grinding of Small Ceramic Elements. *Materials* **2021**, *14*, 7904. [[CrossRef](#)]
24. Denkena, B.; Krödel, A.; Wippermann, A.; Wolters, P. Grinding of transformation-toughened mixed oxide ceramic. *Int. J. Adv. Manuf. Technol.* **2020**, *109*, 1463–1478. [[CrossRef](#)]
25. Wu, S.; Zhang, F.; Ni, Y.; Chen, F.; Yan, Z. Grinding of alumina ceramic with microtextured brazed diamond end grinding wheels. *Ceram. Int.* **2020**, *46*, 19767–19784. [[CrossRef](#)]
26. Pawar, P.; Ballav, R.; Kumar, A. Machining Processes of Silicon Carbide: A Review. *Adv. Mater. Sci.* **2017**, *51*, 62–76.
27. Fedorov, S.V.; Oganyan, G.V. Special features of electron-beam alloying of replaceable polyhedral hard-alloy plates under a complex surface treatment. *Met. Sci. Heat Treat.* **2016**, *57*, 620–624. [[CrossRef](#)]
28. Grigoriev, S.N.; Volosova, M.A.; Okunkova, A.A.; Fedorov, S.V. Influence of Defects in Surface Layer of Al<sub>2</sub>O<sub>3</sub>/TiC and SiAlON Ceramics on Physical and Mechanical Characteristics. *Ceramics* **2023**, *6*, 818–836. [[CrossRef](#)]
29. Grilli, M.L.; Valerini, D.; Slobozeanu, A.E.; Postolnyi, B.O.; Balos, S.; Rizzo, A.; Piticescu, R.R. Critical Raw Materials Saving by Protective Coatings under Extreme Conditions: A Review of Last Trends in Alloys and Coatings for Aerospace Engine Applications. *Materials* **2021**, *14*, 1656. [[CrossRef](#)]
30. Grigoriev, S.; Vereschaka, A.; Zelenkov, V.; Sitnikov, N.; Bublikov, J.; Milovich, F.; Andreev, N.; Mustafaev, E. Specific features of the structure and properties of arc-PVD coatings depending on the spatial arrangement of the sample in the chamber. *Vacuum* **2022**, *200*, 111047. [[CrossRef](#)]
31. Bensouilah, H.; Aouici, H.; Meddour, I.; Yallese, M.A.; Mabrouki, T.; Girardin, F. Performance of coated and uncoated mixed ceramic tools in hard turning process. *Measurement* **2016**, *82*, 1–18. [[CrossRef](#)]
32. Liu, W.; Chu, Q.; Zeng, J.; He, R.; Wu, H.; Wu, Z.; Wu, S. PVD-CrAlN and TiAlN coated Si<sub>3</sub>N<sub>4</sub> ceramic cutting tools—1. Microstructure, turning performance and wear mechanism. *Ceram. Int.* **2017**, *43*, 8999–9004. [[CrossRef](#)]
33. Long, Y.; Zeng, J.; Wu, S. Cutting performance and wear mechanism of Ti–Al–N/Al–Cr–O coated silicon nitride ceramic cutting inserts. *Ceram. Int.* **2014**, *40*, 9615–9620. [[CrossRef](#)]
34. Grigoriev, S.; Vereschaka, A.; Milovich, F.; Tabakov, V.; Sitnikov, N.; Andreev, N.; Sviridova, T.; Bublikov, J. Investigation of multicomponent nanolayer coatings based on nitrides of Cr, Mo, Zr, Nb, and Al. *Surf. Coat. Technol.* **2020**, *401*, 126258. [[CrossRef](#)]
35. Metel, A.S.; Melnik, Y.A.; Panin, V.V. Non-self-sustained glow discharge with electrostatic confinement of electrons sustained by a fast neutral molecule beam. *Plasma Phys. Rep.* **2011**, *37*, 357–365. [[CrossRef](#)]
36. Staszuk, M.; Pakuła, D.; Chladek, G.; Pawlyta, M.; Pancielejko, M.; Czaja, P. Investigation of the structure and properties of PVD coatings and ALD + PVD hybrid coatings deposited on sialon tool ceramics. *Vacuum* **2018**, *154*, 272–284. [[CrossRef](#)]
37. Souza, J.V.C.; Macedo, O.M.; Nono, M.C.A.; Machado, J.P.B.; Pimenta, M.; Ribeiro, M.V. Si<sub>3</sub>N<sub>4</sub> ceramic cutting tool sintered with CeO<sub>2</sub> and Al<sub>2</sub>O<sub>3</sub> additives with AlCrN coating. *Mat. Res.* **2011**, *14*, 514–518. [[CrossRef](#)]
38. Kumar, C.S.; Patel, S.K. Experimental and numerical investigations on the effect of varying AlTiN coating thickness on hard machining performance of Al<sub>2</sub>O<sub>3</sub>-TiCN mixed ceramic inserts. *Surf. Coat. Technol.* **2017**, *309*, 266–281. [[CrossRef](#)]

39. Aslantas, K.; Uçun, İ.; Çicek, A. Tool life and wear mechanism of coated and uncoated Al<sub>2</sub>O<sub>3</sub>/TiCN mixed ceramic tools in turning hardened alloy steel. *Wear* **2012**, *274*, 442–451. [[CrossRef](#)]
40. Grigoriev, S.; Vereschaka, A.; Zelenkov, V.; Sitnikov, N.; Bublikov, J.; Milovich, F.; Andreev, N.; Sotova, C. Investigation of the influence of the features of the deposition process on the structural features of microparticles in PVD coatings. *Vacuum* **2022**, *202*, 111144. [[CrossRef](#)]
41. Wachtman, J.B.; Cannon, W.R.; Matthewson, M.J. *Mechanical Properties of Ceramics*, 2nd ed.; Wiley: Hoboken, NJ, USA, 2009; p. 479, ISBN 978-0-471-73581-6.
42. Zhang, B.; Fu, Y. Grinding of brittle materials with brazed diamond grinding wheel. *Int. J. Adv. Manuf. Technol.* **2013**, *67*, 2845–2852. [[CrossRef](#)]
43. Xiao, X.-L.; Li, G.-X.; Mei, H.-J.; Yan, Q.-S.; Lin, H.-T.; Zhang, F.-L. Polishing of Silicon Nitride Ceramic Balls by Clustered Magnetorheological Finish. *Micromachines* **2020**, *11*, 304. [[CrossRef](#)]
44. Canneto, J.J.; Cattani-Lorente, M.; Durual, S.; Wiskott, A.H.W.; Scherrer, S.S. Grinding damage assessment on four high-strength ceramics. *Dent. Mater.* **2016**, *32*, 171–182. [[CrossRef](#)]
45. Zhang, X.; Kang, Z.; Li, S.; Shi, Z.; Wen, D.; Jiang, J.; Zhang, Z. Grinding force modelling for ductile-brittle transition in laser macro-micro-structured grinding of zirconia ceramics. *Ceram. Int.* **2019**, *45*, 18487–18500. [[CrossRef](#)]
46. Liu, M.H.; Zhang, F.H.; Lu, G.D. Experimental Study of SiC Ceramic Grinding Subsurface Cracks. *Adv. Mater. Res.* **2014**, *1027*, 146–149. [[CrossRef](#)]
47. Andreev, A.A.; Sobol', O.V.; Serdyuk, I.V.; Pinchuk, N.V.; Metel, A.A.; Fedorov, S.V.; Cherkasova, N.Y. Regularities of the influence of the structural state of vacuum-arc-deposited TiN coatings on their resistance to abrasion. *J. Frict. Wear* **2014**, *35*, 497–500. [[CrossRef](#)]
48. Li, Z.; Zhang, F.; Luo, X.; Chang, W.; Cai, Y.; Zhong, W.; Ding, F. Material removal mechanism of laser-assisted grinding of RB-SiC ceramics and process optimization. *J. Eur. Ceram. Soc.* **2019**, *39*, 705–717. [[CrossRef](#)]
49. Bashkov, O.V.; Murav'ev, V.I.; Lonchakov, S.Z.; Frolov, A.V. The research of defects—Stress concentrators by the acoustic emission parameters at the process of damage development. *Izvestiya. Ferrous Metall.* **2015**, *58*, 912–918. [[CrossRef](#)]
50. Sato, N.; Takahashi, K. Evaluation of Fracture Strength of Ceramics Containing Small Surface Defects Introduced by Focused Ion Beam. *Materials* **2018**, *11*, 457. [[CrossRef](#)]
51. Vereschaka, A.S.; Grigoriev, S.N.; Sotova, E.S.; Vereschaka, A.A. Improving the efficiency of the cutting tools made of mixed ceramics by applying modifying nano-scale multilayered coatings. *Adv. Mat. Res.* **2013**, *712–715*, 391–394. [[CrossRef](#)]
52. Vopát, T.; Sahul, M.; Haršáni, M.; Vortel, O.; Zlámal, T. The Tool Life and Coating-Substrate Adhesion of AlCrSiN-Coated Carbide Cutting Tools Prepared by LARC with Respect to the Edge Preparation and Surface Finishing. *Micromachines* **2020**, *11*, 166. [[CrossRef](#)]
53. Vereschaka, A.A.; Vereschaka, A.S.; Grigoriev, S.N.; Kirillov, A.K.; Khaustova, O. Development and research of environmentally friendly dry technological machining system with compensation of physical function of cutting fluids. *Proc. CIRP* **2013**, *7*, 311–316. [[CrossRef](#)]
54. Yushkov, Y.G.; Oks, E.M.; Tyunkov, A.V.; Zolotukhin, D.B. Dielectric Coating Deposition Regimes during Electron-Beam Evaporation of Ceramics in the Fore-Vacuum Pressure Range. *Coatings* **2022**, *12*, 130. [[CrossRef](#)]
55. Matovic, B.; Yano, T. Silicon Carbide and other carbides: From stars to the advanced ceramics. In *Handbook of Advanced Ceramics*; Elsevier: Amsterdam, The Netherlands, 2013; Chapter 3.1; pp. 225–244.
56. Tyunkov, A.; Burdovitsin, V.; Oks, E.; Yushkov, Y.; Zolotukhin, D. An experimental test-stand for investigation of electron-beam synthesis of dielectric coatings in medium vacuum pressure range. *Vacuum* **2019**, *163*, 31–36. [[CrossRef](#)]
57. Wang, P.; Miao, X.; Wu, M.; Zhou, P. Study on the process of abrasive water jet cutting for zirconia ceramic tubes. *Int. J. Adv. Manuf. Technol.* **2023**, *126*, 5555–5569. [[CrossRef](#)]
58. Kogoma, M.; Tanaka, K. Low-temperature atmospheric discharge plasma and its applications for the surface treatment. *Rev. Mod. Plasma Phys.* **2021**, *5*, 3. [[CrossRef](#)]
59. Metel, A.S.; Grigoriev, S.N.; Melnik, Y.A.; Bolbukov, V.P. Characteristics of a fast neutral atom source with electrons injected into the source through its emissive grid from the vacuum chamber. *Instrum. Exp. Tech.* **2012**, *55*, 288–293. [[CrossRef](#)]
60. Grigoriev, S.N.; Melnik, Y.A.; Metel, A.S.; Panin, V.V. Broad beam source of fast atoms produced as a result of charge exchange collisions of ions accelerated between two plasmas. *Instrum. Exp. Tech.* **2009**, *52*, 602–608. [[CrossRef](#)]
61. Grigoriev, S.; Metel, A. Plasma- and Beam-Assisted Deposition Methods. In *Nanostructured Thin Films and Nanodispersion Strengthened Coatings*. NATO Science Series II: Mathematics, Physics and Chemistry; Voevodin, A.A., Shtansky, D.V., Levashov, E.A., Moore, J.J., Eds.; Springer: Berlin, Germany, 2004; Volume 155, pp. 147–154, ISBN 978140202227.394. [[CrossRef](#)]
62. Metel, A.S.; Melnik, Y.A. A high-current plasma emitter of electrons based on a glow discharge with a multirod electrostatic trap. *Instrum. Exp. Tech.* **2013**, *56*, 317–324. [[CrossRef](#)]
63. Arif, M.; Sauer, M.; Foelske-Schmitz, A.; Eisenmenger-Sittner, C. Characterization of aluminum and titanium nitride films prepared by reactive sputtering under different poisoning conditions of target. *J. Vacuum Sci. Technol. A* **2017**, *35*, 061507. [[CrossRef](#)]
64. Glazunov, V.N.; Metel', A.S. Inversion of cathode cavity of glow discharge in a magnetic field. *Sov. Phys. Tech. Phys.* **1981**, *26*, 559–562.

65. Jeon, Y.; Park, Y.S.; Kim, H.J.; Hong, B.; Choi, W.S. Tribological properties of ultrathin DLC films with and without metal interlayers. *J. Korean Phys. Soc.* **2007**, *51*, 1124–1128. [[CrossRef](#)]
66. Wang, K.; Zhou, H.; Zhang, K.; Liu, X.; Feng, X.; Zhang, Y.; Chen, G.; Zheng, Y. Effects of Ti interlayer on adhesion property of DLC films: A first principle study. *Diam. Relat. Mater.* **2021**, *111*, 108188. [[CrossRef](#)]
67. Grigoriev, S.N.; Volosova, M.A.; Vereschaka, A.A.; Sitnikov, N.N.; Milovich, F.; Bublikov, J.I.; Fyodorov, S.V.; Seleznev, A.E. Properties of (Cr,Al,Si)N-(DLC-Si) composite coatings deposited on a cutting ceramic substrate. *Ceram. Int.* **2020**, *46*, 18241–18255. [[CrossRef](#)]
68. Kiryukhantsev-Korneev, P.V.; Phiri, J.; Gladkov, V.I.; Ratnikov, S.N.; Yakovlev, M.G.; Levashov, E.A. Erosion and Abrasion Resistance, Mechanical Properties, and Structure of the TiN, Ti–Cr–Al–N and Cr–Al–Ti–N Coatings Deposited by CFUBMS. *Prot. Met. Phys. Chem. Surf.* **2019**, *55*, 913–923. [[CrossRef](#)]
69. Sytchenko, A.D.; Vakhrushev, R.A.; Kiryukhantsev-Korneev, P.V. Investigation of the tribological characteristics of Ta–Zr–Si–B–C–N coatings. *Powder Metall. Funct. Coat.* **2023**, *17*, 62–70.
70. Lesnevskiy, L.N.; Lyakhovetskiy, M.A.; Savushkina, S.V. Fretting wear of composite ceramic coating produced on D16 aluminum-based alloy using microarc oxidation. *J. Frict. Wear* **2016**, *37*, 268–273. [[CrossRef](#)]
71. Betsofen, S.Y.; Rokhlin, L.L.; Wu, R.; Lozovan, A.A.; Voskresenskaya, I.I. Effect of alloying elements on the texture and the anisotropy of the mechanical properties of magnesium alloys with REM, lithium, and aluminum. *Russ. Metall.* **2014**, *11*, 920–927. [[CrossRef](#)]
72. Metel, A.; Melnik, Y.; Mustafaev, E.; Minin, I.; Pivkin, P. Combined Processing of Micro Cutters Using a Beam of Fast Argon Atoms in Plasma. *Coatings* **2021**, *11*, 465. [[CrossRef](#)]
73. Bortoleto, J.R.R.; Chaves, M.; Rosa, A.M.; da Silva, E.P.; Durrant, S.F.; Trino, L.D.; Lisboa-Filho, P.N. Growth evolution of self-textured ZnO films deposited by magnetron sputtering at low temperatures. *Appl. Surf. Sci.* **2015**, *334*, 210–215. [[CrossRef](#)]
74. Avila, P.R.T.; da Silva, E.P.; Rodrigues, A.M.; Aristizabal, K.; Pineda, F.; Coelho, R.S.; Garcia, J.L.; Soldera, F.; Walczak, M.; Pinto, H.C. On manufacturing multilayer-like nanostructures using misorientation gradients in PVD films. *Sci. Rep.* **2019**, *9*, 15898. [[CrossRef](#)]
75. Severin, S.; Naveed, M.; Weiß, S. Effect of HPPMS Pulse-Frequency on Plasma Discharge and Deposited AlTiN Coating Properties. *Adv. Mater. Sci. Eng.* **2017**, *2017*, 4850908. [[CrossRef](#)]
76. Tonshoff, H.K.; Karpuschewski, B.; Mohlfeld, A.; Seegers, H. Influence of subsurface properties on the adhesion strength of sputtered hard coatings. *Surf. Coat. Technol.* **1999**, *114*, 524–529. [[CrossRef](#)]
77. Yanga, J.; Odénb, M.; Johansson-Jöesaarb, M.P.; Llanesa, L. Grinding Effects on Surface Integrity and Mechanical Strength of WC-Co Cemented Carbides. *Proc. CIRP* **2014**, *13*, 257–263. [[CrossRef](#)]
78. Krella, A. Resistance of PVD Coatings. Encyclopedia. Available online: <https://encyclopedia.pub/entry/2419> (accessed on 11 October 2023).
79. Kübarsepp, J.; Juhani, K.; Tarraste, M. Abrasion and Erosion Resistance of Cermets: A Review. *Materials* **2022**, *15*, 69. [[CrossRef](#)]
80. Renz, A.; Khader, I.; Kailer, A. Tribochemical wear of cutting-tool ceramics in sliding contact against a nickel-base alloy. *J. Eur. Ceram. Soc.* **2016**, *36*, 705–717. [[CrossRef](#)]
81. Osmond, L.; Cook, I.; Slatter, T. Tribological Properties of Multilayer CVD Coatings Deposited on SiAlON Ceramic Milling Inserts. *J. Manuf. Mater. Process.* **2023**, *7*, 67. [[CrossRef](#)]

**Disclaimer/Publisher’s Note:** The statements, opinions and data contained in all publications are solely those of the individual author(s) and contributor(s) and not of MDPI and/or the editor(s). MDPI and/or the editor(s) disclaim responsibility for any injury to people or property resulting from any ideas, methods, instructions or products referred to in the content.